Tracing silicate weathering processes in the permafrost-dominated Lena River watershed using lithium isotopes

Melissa J. Murphy[*a], Don Porcelli[a], Philip A.E. Pogge von Strandmann[b], Catherine A. Hirst[c,d], Liselott Kutscher[c,e], Joachim A. Katchinoff[f], Carl-Magnus Mörth[e], Trofim Maximov[g], Per S. Andersson[c]

a Department of Earth Sciences, University of Oxford, South Parks Road, Oxford OX1 3AN, UK.

b London Geochemistry and Isotope Centre (LOGIC), Institute of Earth and Planetary Sciences, University College London and Birkbeck College, Gower Street, London, WC1E 6BT, UK.

c Department of Geosciences, Swedish Museum of Natural History, Box 50007, SE-104 05 Stockholm, Sweden.

d Earth and Life Institute, Université catholique de Louvain, Croix du Sud, L7.05.10, B-1348 Louvain-la-Neuve, Belgium

e Department of Geological Sciences, Stockholm University, SE-10691 Stockholm, Sweden.

f Department of Geology & Geophysics, Yale University, USA.

g Institute for Biological Problems of the Cryolithozone, Siberian Branch, Russian Academy of Science, Russia.

*Corresponding author: Now at: London Geochemistry and Isotope Centre (LOGIC), Institute of Earth and Planetary Sciences, University College London and Birkbeck College, Gower Street, London, WC1E 6BT, UK. Email address: melissa.murphy@ucl.ac.uk

Abstract

Increasing global temperatures are causing widespread changes in the Arctic, including permafrost thawing and altered freshwater inputs and trace metal and carbon fluxes into the ocean and atmosphere. Changes in the permafrost active layer thickness can affect subsurface water flow-paths and water-rock interaction times, and hence weathering processes. Riverine lithium isotope ratios (reported as δ^7Li) are tracers of silicate weathering that are unaffected by biological uptake, redox, carbonate weathering and primary lithology. Here we use Li isotopes to examine silicate weathering processes in one of the largest Russian Arctic rivers: the Lena River in eastern Siberia. The Lena River watershed is a large multi-lithological catchment, underlain by continuous permafrost. An extensive dataset of dissolved Li isotopic compositions of waters from the Lena River main channel, two main tributaries (the Aldan and Viliui Rivers) and a range of smaller sub-tributaries are presented from the post-spring flood/early-summer period at the onset of active layer development and enhanced water-rock interactions. The Lena River main channel (average δ^7Li_{diss} ~19‰) has a slightly lower isotopic composition than the mean global average of 23‰ (Huh et al., 1998a). The greatest range of [Li] and δ^7Li_{diss} are observed in catchments draining the south-facing slopes of the Verkhoyansk Mountain Range. South-facing slopes in high-latitude, permafrost-dominated regions are typically characterised by increased summer insolation and higher daytime temperatures relative to other slope aspects. The increased solar radiation on south-facing catchments promotes repeated freeze-thaw cycles, and contributes to more rapid melting of snow cover, warmer soils, and increased active layer thaw depths. The greater variability in δ^7Li and [Li] in the south-facing rivers likely reflect the greater infiltration of melt water and enhanced water-rock interactions within the active layer.

A similar magnitude of isotopic fractionation is observed between the low-lying regions of the Central Siberian Plateau (and catchments draining into the Viliui River), and catchments draining the Verkhoyansk Mountain Range into the Aldan River. This is in contrast to global rivers in non-permafrost terrains that drain high elevations or areas of rapid uplift, where high degrees of physical erosion promote dissolution of freshly exposed primary rock typically yielding low δ^7Li_{diss}, and low-lying regions exhibit high riverine δ^7Li values resulting from greater water-rock interaction and formation of secondary mineral that fractionates Li isotopes. Overall, the range of Li concentrations and δ^7Li_{diss} observed within the Lena River catchment are comparable to global rivers located in temperate and tropical regions. This suggests that cryogenic weathering features specific to permafrost regions (such as the continual exposure of fresh primary minerals due to seasonal

freeze-thaw cycles, frost shattering and salt weathering), and climate (temperature and runoff), are not a dominant control on δ^7Li variations. Despite vastly different climatic and weathering regimes, the same range of riverine δ^7Li values globally suggests that the same processes govern Li geochemistry – that is, the balance between primary silicate mineral dissolution and the formation (or exchange with) secondary minerals. This has implications for the use of δ^7Li as a palaeo-weathering tracer for interpreting changes in past weathering regimes.

1. Introduction

Permafrost thawing in high-latitude polar regions that is induced by climate warming influences mineral, elemental, nutrient and carbon fluxes (dissolved and particulate) into the ocean and atmosphere. Changes in the permafrost active layer thickness dictate subsurface water flowpaths, as well as water-rock interaction times and hence weathering processes, and this may impact future terrestrial biogeochemical cycles (Frey and McClelland, 2009). The evolution of long-term climate is influenced by the supply of cations from silicate weathering (providing alkalinity, which sequesters CO_2 by carbonate precipitation in the oceans), as well as by delivering nutrients that facilitate organic carbon burial (Walker et al., 1981; Berner et al., 1983). To date, however, understanding the influence of climatic (e.g., temperature and runoff) and physical rock supply (e.g., sediment supply, physical erosion) controls on weathering are uncertain and highly debated (e.g., Raymo and Ruddiman, 1992; West et al., 2005; Hilley et al., 2010; Eiriksdottir et al., 2013). Changes in silicate weathering are in turn predicted to have significantly affected long- and short-term climate perturbations in the past (Raymo et al., 1988; Raymo and Ruddiman, 1992; Pogge von Strandmann et al., 2013).

Water-rock interactions, and hence silicate weathering, in cold-climate regions differ from those of warm and wet watersheds in temperate and tropical regions. The latter tend to be characterised by transport- or supply-limited regimes, where weathering rates are limited by the supply of fresh primary minerals. At low erosion rates, primary minerals are nearly completely altered, and the rate of secondary mineral formation exceeds that of primary mineral dissolution. This allows for the accumulation of thick soil profiles and long water-rock interaction times. In high erosion kinetically-limited weathering environments, the rate of chemical weathering is limited relative to physical erosion. Soil production is limited because physical erosion removes weathered material rapidly preventing significant accumulation of secondary minerals, resulting in shorter water-rock interaction times (Stallard and Edmond, 1983; West et al., 2005).

In high-latitude or alpine regions, low mean annual temperatures are expected to inhibit mineral reaction rates, resulting in incomplete weathering of silicate material (West et al., 2005). Nonetheless, it has been proposed that high rates of physical erosion from frost action and salt weathering, and enhanced primary rock dissolution by organic acids, can promote greater chemical weathering than might otherwise be expected in high-latitude regions dominated by temperature-controlled slow reaction rates (Gislason et al., 1996; Nezat et al., 2001; Huh, 2003).

Most weathering processes observed in weathering regimes in tropical and temperate climates are also prevalent in regions underlain by permafrost. However, the presence of permafrost further complicates water-rock interactions at high altitude and polar regions. Permafrost underlies nearly a quarter of the northern hemisphere, and underlies approximately 90% of the Lena River catchment, NE Siberia (Brown et al., 1997). Rivers in permafrost-dominated regions have very different hydrologic regimes to rivers in non-permafrost areas. In continuous permafrost-dominated catchments, perennially frozen soil/bed rock inhibits infiltration of surface water, thereby restricting subsurface water storage and limiting water-rock interactions. Rapid melting of winter precipitation (snow) accumulated within the catchment over ~8 to 9 months results in the high runoff spring freshet, which flows over the still frozen permafrost. In early spring, increasing air temperatures promote thawing of the near-surface and development of the 'active layer'. This enables water infiltration into the uppermost shallow (often organic-rich) thawed soil, and water is temporarily stored as ponded surface waters perched above the permafrost in low-lying wetlands and fens. Throughout the summer and early autumn before refreezing occurs, the active layer thaws to its maximum depth, potentially promoting exposure of more readily weathered rocks, deepening of flow paths and allowing greater water interaction with mineral-rich soil horizons (Woo, 2012). Unlike in tropical and temperate regions, the majority of hydrological processes (and hence silicate weathering) in permafrost-dominated terrains occurs within the seasonally thawed active layer (and regions of unfrozen talik) over the short thaw period. Rivers in watersheds with higher permafrost coverage tend to have lower subsurface storage capacity and thus a lower winter base flow and a higher summer peak flow compared to non-permafrost rivers (Ye et al., 2009; Woo, 2012).

In principle, climate warming could drive large annual changes in both the rate of silicate weathering and the weathering regime by contraction of the area underlain by continuous permafrost, increasing active layer thickness, and allowing greater suprapermafrost and talik groundwater flow (Frey and McClelland, 2009). This could affect the biogeochemical cycles of many

121 elements and the supply of micronutrients to northern oceans. It could also impact the Earth's
122 climate feedback cycles through the release of carbon trapped within permafrost into the
123 atmosphere and oceans. Since the response of weathering processes to permafrost thawing is not
124 well understood (Pokrovsky et al., 2005; Frey et al., 2007; Frey and McClelland, 2009; Keller et al.,
125 2010), it is unknown whether carbon removal via silicate weathering or carbon release from
126 permafrost thawing will have the greatest effect on the carbon budget. Constraining the processes
127 that govern silicate weathering in high-latitude, permafrost dominated regions is therefore critical
128 for quantifying the global carbon cycle over modern and geological timescales.
129 To date, it has proven difficult to constrain weathering processes at any scale, particularly in
130 permafrost-dominated regions, because most tracers that are used are affected by multiple
131 processes (e.g. biology, lithology, redox, etc.). Riverine lithium isotope ratios ($^{7}Li/^{6}Li$, reported as
132 $\delta^{7}Li$, that is the permil deviation from the $^{7}Li/^{6}Li$ ratio of the L-SVEC standard) trace silicate
133 weathering processes at scales ranging from soils and small monolithological catchments to
134 significant global river watersheds that integrate large areas of variable lithology and often several
135 climatic regions. Lithium isotopes are not fractionated in the environment by biological processes
136 (Lemarchand et al., 2007; Pogge von Strandmann et al., 2016). Also, Li is orders of magnitude more
137 concentrated in silicates over carbonates, so that even in carbonate catchments, Li isotopes are
138 dominated by silicate weathering (Kısakűrek et al., 2005; Millot et al., 2010). River $\delta^{7}Li$ values are
139 controlled by what has been described as "silicate weathering congruency" (Misra and Froelich,
140 2012; Pogge von Strandmann and Henderson, 2015; Vigier and Goddéris, 2015; Pogge von
141 Strandmann et al., 2016; 2017). This is defined as the ratio of primary mineral dissolution (releasing
142 largely unfractionated Li with crustal $\delta^{7}Li$ ~0 to 5‰) to secondary mineral formation (which
143 preferentially incorporate ^{6}Li, increasing the $\delta^{7}Li$ composition of Li remaining in solution; (Pistiner
144 and Henderson, 2003; Vigier et al., 2008; Wimpenny et al., 2010a). High riverine $\delta^{7}Li$ values have
145 been interpreted as reflecting less complete weathering, greater secondary mineral formation and
146 thus greater 'weathering intensity' (i.e., the ratio of chemical to physical denudation; Bouchez et al.,
147 2013; Dellinger et al., 2015). There have been a number of large global rivers in tropical and
148 temperate environments where the behaviour of Li isotopes has been studied: e.g., the Amazon
149 River (Chan et al., 1992; Huh et al., 1998a; Dellinger et al., 2014, 2015); the Orinoco River (Huh et
150 al., 1998a; Huh et al., 2001); rivers in the High Himalayas and the Ganges-Brahmaputra (Huh et al.,
151 1998a; Kısakűrek et al., 2005; Bagard et al., 2015; Manaka et al., 2017; Pogge von Strandmann et
152 al., 2017) the Changjiang (Yangtzee) River (Huh et al., 1998a; Liu et al., 2011; Wang et al., 2015); the

Mississippi River (Chan et al., 1992; Huh et al., 1998a) and the Congo River (Henchiri et al., 2016). However, there are fewer studies of rivers draining cold climate regions. Whilst some data from Siberia exist, the sampling sites are limited to a handful of locations from the major tributaries and river mouths (Huh et al., 1998a). The only comparable studies of high-latitude polar regions are the Mackenzie River basin (Millot et al., 2010) and the comparatively short rivers of Iceland (Pogge von Strandmann et al., 2006; Vigier et al., 2009; Pogge von Strandmann et al., 2016), Greenland (Wimpenny et al., 2010b), the McMurdo Dry Valleys in Antarctica (Witherow et al., 2010), and Svalbard (Hindshaw et al., 2018).

In this study, Li isotopic compositions were measured in over 70 river samples and 11 suspended sediments across the catchment of the vast and relatively unstudied Lena River in eastern Siberia. The multi-lithological catchment spans a latitudinal and climate gradient from 60° to 68° N and is largely underlain by continuous permafrost. The effects of secondary mineralogy, climate, topography and presence of permafrost on silicate weathering are investigated. This study vastly increases the amount of Li isotope data from high latitudes, which has been limited partly due to difficulties in logistics and gaining access.

2. Background

2.1 Study Area

The Lena River basin is located in Yakutia in eastern Siberia (Fig. 1). The Lena River is one of the largest Russian Arctic rivers, draining a watershed area of 2.46 x 10^6 km^2. The river flows northwards from 53°N near Lake Baikal to 71°N and enters the Arctic Ocean in the Laptev Sea. The headwaters originate in the discontinuous and patchy mountain permafrost of the Baikal, Stanovoi and Dzhugdzhur mountains. Northward from 60°N latitude, the Lena River watershed is underlain by variable thicknesses of continuous permafrost ranging from 50 meters to over 1500 m (Brown et al., 1997; (Chevychelov and Bosikov, 2010)). The seasonally thawed active layer varies in thickness throughout the catchment from a few centimetres to several meters (Huh et al., 1998c). The Lena River contributes approximately 15% of the total freshwater input into the Arctic Ocean, of which ~85% is provided during the spring flood and summer months (May – September; Ye et al., 2003). The geology of eastern Siberia has been described in detail by Gordeev and Sidorov, (1993), Huh et al. (1998b, 1998c), and Huh and Edmond, (1999). Briefly, the Central Siberian Plateau (CSP; see Fig. 1) is underlain by Proterozoic crystalline and metamorphic basement of the stable Siberian Platform, which outcrop to the south in the mountainous Trans-Baikal region where the headwaters of the

Lena River form, and to the east in the Archean Aldan-Stanovoy shield mountains which are drained by rivers in the Lena-Amginsky inter-river area (LAIRA). The CSP is typified by gentle topography and extensive flood plains, with thick sedimentary cover composed of Precambrian to Quaternary marine carbonates and evaporites, along with terrigenous sandstone, shale, red beds, and coal beds. The Verkhoyansk Mountain Range forms a topographic high to the east and is composed of folded and metamorphosed rocks and uplifted detrital sediments. It is not actively undergoing tectonic uplift.

The climate of the watershed is continental, characterised by long cold winters and short, hot summers, with temperatures ranging from −50 °C to +35 °C. The mean annual air temperature (MAAT) ranges from −6 to −15°C across the region and decreases with increasing latitude (Fedorov et al., 2014). The mean annual precipitation (MAP) is typically low, ranging from 200 to 500 mm/yr (Chevychelov and Bosikov, 2010). The drainage area is mainly composed of boreal taiga forest of larch and salix in the southern parts of the basin, with exposed rock outcrops, small shrubs, moss and lichen in the tundra regions of the northern part of the basin (Gordeev and Sidorov, 1993).

3. Analytical methods

3.1 Field sampling

The samples and methods are described in detail by Hirst et al. (2017) and Kutscher et al. (2017). Briefly, sampling occurred over two field campaigns (summer of July 2012 and late spring/early summer of June 2013) when the active layer is thickest and so suprapermafrost groundwater flow is deepest. Sampling dates, locations and descriptions are given in Fig. 1 and Table S1. In the field, surface water samples were collected in acid-washed 10 L low density polyethylene (LDPE) bottles by grab sampling from the upstream side of the ship or small motorised boat, or by wading out into river channels. Samples were filtered within a few hours using a polycarbonate Geotech® filter holder and 0.22 µm nitrocellulose filters (Millipore®) prewashed with 5% acetic acid and ultrapure Milli-Q water. At each sampling locality, pH, temperature and electrical conductivity were measured *in-situ* using a multi-meter (YSI 556 multiprobe system) with analytical accuracies of ± 0.03 pH units, ± 0.1 °C, and ± 1 µS/cm.

The rivers for this study have been geographically grouped according to Kutscher et al. (2017): (i) the Lena River main channel; (ii) the low-lying Central Siberian Plateau (CSP) tributaries; (iii) the main channel of the major Viliui River tributary that is sourced from that region; (iv) the mountainous tributaries draining the Verkhoyansk Mountain Range (VMR); (v) the main channel of

217 the major Aldan River tributary; and (vi) tributaries draining the Lena-Amginsky inter-river area
218 (LAIRA).
219
220 ***3.2*** *Major cation and trace element analyses*
221 Major cations were measured by Inductively Coupled Plasma Optical Emission Spectroscopy (ICP-
222 OES Thermo Icap 6500 Duo) at the Department of Geological Sciences, Stockholm University. For
223 details, see Sun et al. (2018). For the majority of samples, Li concentrations were analysed using an
224 Element 2 sector-field Inductively-Coupled-Plasma Mass Spectrometer (ICP-MS) at the University of
225 Oxford. For Li analyses, standard addition calibration curves were prepared by doping a given
226 sample with a multi-elemental standard solution (Alfa Aesar®) to account for matrix effects. Both
227 standard and water samples were doped with 1 ng/g of rhenium internal standard to correct for
228 instrumental drift. Accuracy was assessed by analysing IAPSO seawater and the international river
229 reference standard SLRS-5, and by measuring samples in duplicate, and external analytical
230 uncertainties were better than 5%. For a handful of samples with Li concentrations below the limit
231 of detection on the Element 2 (<60 nM Li, see Table 1), concentrations were estimated by intensity
232 matching against a known concentration of L-SVEC on the MC-ICP-MS (see below), with
233 uncertainties estimated to be ± 10%.
234
235 ***3.3*** *Li isotope measurements*
236 For Li isotope analysis of the waters, a sufficient volume of each sample was evaporated to yield 10-
237 20 ng Li, and refluxed 1-2 times with concentrated HNO_3 to break down organics prior to separation.
238 This stage is necessary in these organic-rich samples, and resulted in an improvement of internal
239 precision on the measurements by *ca.* 50%. For the suspended sediments, filters were digested
240 using protocols outlined by (Hirst et al., 2017). Evaporated water samples and aliquots of the filter
241 digests were dissolved in 0.2 M HCl and passed through a two-stage cation exchange
242 chromatography procedure (BioRad® AG50W-X12), using dilute HCl as an eluent (Pogge von
243 Strandmann et al., 2011; Pogge von Strandmann and Henderson, 2015). In order to confirm that
244 quantitative Li yields on the column were achieved and no significant fractionation occurred on the
245 column, aliquots before and after the main elution were analysed. Blanks for the total chemical
246 procedure were less than 5 pg Li, which is negligible relative to the 10–20 ng of Li analysed in each
247 sample.

Lithium isotope compositions were determined on a Nu Plasma HR-MC-ICP-MS at the Department of Earth Sciences, University of Oxford, in dry plasma mode using a Cetac Aridus-II desolvating system. Corrections for instrumental mass bias were made using sample-standard bracketing. Data are reported in δ^7Li notation, the permil deviation of the measured ^{7}Li/^{6}Li ratio from the L-SVEC standard (NIST SRM 8545; Flesch et al., 1973), where $\delta^7Li = [(^7Li/^6Li_{sample})/ (^7Li/^6Li_{L\text{-}SVEC})\text{-}1] \times 1000$. Each sample was analysed in triplicate during the course of each run. Individual errors are the two standard deviation around the mean of at least two, but typically three, replicate measurements. The external reproducibility was determined by repeat measurements of an internal seawater standard processed through the full chemical procedure, which yielded δ^7Li = 31.3 ± 0.7‰ (2sd; n = 20). Two rock standards were also run, granite JG-2 (δ^7Li = 0.4 ± 0.2‰, n=3) and Wyoming oil shale SGR-1b (δ^7Li = 3.6 ± 0.4‰, n=3), and the results are within uncertainty of other published values (Pogge von Strandmann et al., 2017 and references therein). Replicates of samples processed in duplicate (n = 9 waters, 3 sediments) in different analytical sessions are indistinguishable from one another within analytical error, with the exception of LR2012-37, which shows slightly greater variability (1.5‰; Table 1). Duplicates are plotted as the average of the two measurements.

4. Results

Sample location and field parameter data (from Hirst et al. 2017; Kutscher et al. 2017), dissolved [Na] and [Li] (where square brackets denote concentrations), δ^7Li_{diss} and suspended sediment δ^7Li_{susp} are given in Table 1. Other major elemental data are presented in Sun et al. (2018). Lithium concentrations range from 12 to 1520 nM. This range is similar to that observed from long-term seasonal monitoring of the Lena River at Zhigansk (Fig. 1, [Li] = 115 to 628 nM; Holmes et al., 2018). Dissolved δ^7Li values range between +7.1 and +41.9‰ (Fig. 2). Despite the large range of values, the average δ^7Li_{diss} for the geographical regions vary within only a few permil. Average [Li] and δ^7Li_{diss} compositions are presented as box-and whisker plots in Supplementary Fig. 1 to show the distribution of data. Lithium concentrations within the Lena River main channel (average ~134 nM) are lower than the global mean of 215 nM, and are similar to shield-draining rivers elsewhere (Huh et al., 1998a). The Viliui River as well as the tributaries of the CSP, LAIRA and VMR have higher average [Li] (232 to 338 nM) when compared to the Lena River main channel and Aldan River. The greatest ranges in both [Li] and δ^7Li are observed in rivers draining the Verkhoyansk Mountain Range (VMR), and especially in catchments that predominantly have a south-facing aspect (See Fig. 1 and Table 1). Overall, the data presented here are comparable with the more limited previously

published data in the Lena River catchment ([Li] = 40 to 3350 nM; δ^7Li = 19.0 to 29.9‰; Huh et al., 1998a). The furthest downstream sample from this study (LR2013-45, [Li] = 192 nM, δ^7Li = 21.3‰) is indistinguishable to sample UL607 from the Lena River outflow ~500 km at Kusur measured previously ([Li] = 220 nM, δ^7Li = 21.5‰; Huh et al., 1998a). Both samples LR2013-45 and UL607 were collected during the early summer months (in June 2013 and July 1995, respectively).

Using published monthly discharge and [Li] data from R-ArcticNet (http://www.r-arcticnet.sr.unh.edu/v4.0/index.html), ArcticRIMS (http://rims.unh.edu/data.shtml) and the Arctic Great Rivers Observatory (http://arctic greaterivers.org/data.html), an annual discharge-weighted Li flux into the Arctic Ocean of 1.29×10^8 mol/yr can be calculated. Using a [Li] = 192 nM of our northernmost sample (LR2013-45) and the average annual discharge, we obtain an annual flux of 1.03×10^8 mol/yr, which is comparable to the estimate of 1.18×10^8 mol/yr by Huh et al. (1998a). This accounts for approximately 1% of the global riverine Li flux into the ocean.

The Li isotopic composition of the Lena River main channel is relatively uniform throughout the catchment (~19 ± 2‰; 1σ), and is several permil lower than the global riverine mean of ~23‰ (Huh et al., 1998a), with the exception of one atypical sample with high [Li] and δ^7Li (LR2013-41; δ^7Li = 29.0‰, 396 nM). The ranges of δ^7Li and [Li] measured in this study are similar to those of data from other large global rivers systems elsewhere (e.g., the Mackenzie River, Millot et al., 2010; the Ganges-Brahmaputra, Kısakűrek et al., 2005, Bagard et al., 2015, Pogge von Strandmann et al., 2017; and the Amazon, Dellinger et al., 2015).

The rivers in the Lena catchment show a broad positive trend between δ^7Li_{diss} and 1/[Li], although the lack of a simple relationship between δ^7Li and Li concentration for the Lena River main channel and the main catchment regions (Fig. 2) indicates that there are a range of processes controlling the Li concentrations and isotope variations. In particular, the data cannot be adequately explained by simple mixing between two endmembers with different isotopic compositions and weathering regimes, as has been inferred for the Mackenzie River Basin (Millot et al., 2010) and the Congo River (Henchiri et al., 2016). This is not unexpected in such a large complex, multi-lithological drainage region.

Four sets of samples were collected from the same locations in both the July 2012 and June 2013 field campaigns (Table 1; LR2012-23/LR2013-77 and LR2012-24/LR2013-76 from a tributary draining the VMR; LR2012-03/LR2013-78 from the main channel of the Lena River; and LR2012-22/LR2013-38 from the Aldan River). With the exception of the LR2012-24/LR2013-76 pair of samples, which had similar [Li] , the concentrations of samples collected in 2013 were almost double

those of their 2012 counterparts. In all instances, however, the δ^7Li values of the samples from the same locations sampled during both campaigns were within 1-2‰ of one another. This might suggest that despite presumed increases in the thickness of the active layer during the warmer months, there is only limited δ^7Li variation.

The suspended sediments have a narrow δ^7Li_{susp} range from +0.4 to +5.1‰ (Supplementary Fig. 2), which broadly overlaps with average continental silicate rock values (UCC, ~ 0.6 ± 0.6‰, Teng et al., 2004; Sauzéat et al., 2015; and basalts ~3 to 5‰, Elliott et al., 2006, Tomascak et al., 2008). The suspended sediments are isotopically heavier than the global mean suspended sediment Li isotopic composition for large global rivers of -1.5 ± 1‰ (1σ; Dellinger et al., 2014) but comparable to δ^7Li_{susp} values for other rivers (e.g., the Mackenzie River, Millot et al. 2010; the Ganges-Brahmaputra; Kısakűrek et al. 2005, Bagard et al. 2015, Pogge von Strandmann et al. 2017; the Dongqu, Weynell et al., 2017); and the Amazon, Dellinger et al., 2014). Variations in δ^7Li have been reported for suspended sediments related to variations in Si/Al (a proxy for grain size) in depth profiles in the Amazon, Mackenzie and Ganges-Brahmaputra Rivers that are the result mineral sorting within the water column (Bouchez et al. 2011, Dellinger et al. 2014, (Dellinger et al., 2014). However, only suspended sediments from near-surface waters have been collected in this study, and the use of HF in the filter dissolution protocol in these samples precludes the use of Si/Al as a proxy for grain size.

The isotopic offset between δ^7Li_{susp} and δ^7Li_{diss} ($\Delta^7Li_{susp\text{-}diss} = \delta^7Li_{susp} - \delta^7Li_{diss}$) for the different geographical regions within the Lena River watershed generally varies between 12.5 and -22.6 ‰ (shown in Supplementary Fig. 3). With the exception of the south-facing VMR sample with $\Delta^7Li_{susp\text{-}diss}$ = -34.3‰, the narrow range of values do not allow for discrimination between the geographical regions. The magnitude of $\Delta^7Li_{susp\text{-}diss}$ observed within the Lena River is comparable to values observed in rivers elsewhere ($\Delta^7Li_{susp\text{-}diss}$ = -6 to -36 ‰; Huh et al., 2001; Kısakűrek et al., 2005; (Pogge von Strandmann et al., 2006; Pogge von Strandmann et al., 2010).

5. Discussion

The fractionation of Li isotopes is controlled by water-rock interactions during weathering processes, specifically the balance between release of Li during primary silicate rock dissolution, and the preferential incorporation or adsorption of ^6Li during formation of secondary minerals (Pistiner and Henderson, 2003; Vigier et al., 2008; Wimpenny et al., 2010a). The variations in δ^7Li_{diss} across the Lena River catchment reflect numerous complex processes occurring over the

watershed. The lack of detailed observational data on the thermal regime for the individual catchment regions (e.g., active layer thaw depths, local microclimate, snow conditions, vegetation, soil properties, moisture content, lateral drainage, ground ice, etc.; Woo, 2012) complicates the interpretation of these isotopic variations to specific permafrost conditions. Here, we attempt to distinguish the dominant processes controlling Li isotope fractionation over such a large, complex, permafrost-dominated watershed.

5.1 *Sources of dissolved lithium*

Although carbonate weathering is the dominant contributor to total dissolved solids (TDS) in the Lena River catchment (Huh et al., 1998c; Huh et al., 1998b; Huh and Edmond, 1999), it contributes only a small fraction of the dissolved Li due to the low [Li] in carbonates. The possibility of inputs of Li from rainwater, ultimately derived from sea spray and so accompanied by other elements in the same proportions as in seawater, was investigated using the methods of Millot et al. (2010) and Dellinger et al. (2014) and a rainwater [Cl] after Gordeev et al. (1996). The range of measured Li/Cl ratios (1.6×10^{-4} to 7.9×10^{-2}) is much higher than the seawater ratio of 5×10^{-5}, and so a negligible (<5%) proportion of riverine Li originates from precipitation. Thus, the δ^7Li data have not been corrected for these inputs, consistent with the approaches of other riverine studies (e.g. Millot et al., 2010; Bagard et al., 2015; Liu et al., 2015; Pogge von Strandmann et al., 2017).

Some of the rivers draining the CSP have elevated [Cl] and [$SO4^-$], which might be derived from weathering of evaporites that are abundant within the catchment region (Gordeev and Sidorov, 1993; Huh et al., 1998c; Yoon, 2010). However, as noted by Yoon, (2010), this may also reflect a contribution from high [Cl] and [$SO4^-$] groundwaters. Using the same approach as Dellinger et al. (2014), and assuming evaporites have Li/Na = 3×10^{-5}, a low evaporite contribution has only been identified for a number of CSP (LR2013-50 (3%), LR2013-68 (8%), LR2013-79 (9%), LR2013-72 (5%)); and Lena River main channel samples (LR2012-30, LR2012-32 and LR2013-48 (~5%); LR2012-31, LR2012-34 and LR2013-49 (~6%)). Overall, the calculations show that dissolved Li is dominantly derived from the weathering of silicate material.

5.2 *Secondary mineralogical controls on Li isotope fractionation - Mineral saturation states*

The large range of Li isotope ratios observed in rivers has been proposed to reflect mineral-specific isotope fractionation factors controlled by the precipitation of (or interaction with) different secondary mineral assemblages. This has been attributed to differences in bedrock lithology as well

as weathering regime and hence weathering intensity, which control the water chemistry by removing major and trace elements from solution as the various secondary mineral phases precipitate (e.g., Millot et al., 2010; Wimpenny et al., 2010b; Pogge von Strandmann et al., 2006, 2010).

In order to assess the likelihood and mineralogy of secondary mineral formation in the studied rivers, mineral saturation states were calculated with PHREEQC (Parkhurst and Appelo, 1999), using the measured dissolved major cation and anion, Al and Fe concentrations, and *in-situ* pH, alkalinity and temperature data (after Hirst et al. 2017 and Sun et al. 2018). The PHREEQC calculations indicate that in river samples from all of the geographical regions within the Lena River watershed, primary minerals such as quartz, olivine, pyroxene and feldspar are undersaturated and so are likely to be dissolving. In contrast, secondary minerals that are oversaturated (SI >0) in all rivers (and hence are likely to be precipitating) include amorphous and crystalline Fe oxyhydroxides (e.g., goethite, hematite, magnetite), Al oxides (e.g., gibbsite), Mn oxides (e.g., birnessite) and phyllosilicate minerals (e.g., K-mica, kaolinite, pyrophyllite). Smectite clay minerals (Ca- and Na-montmorillonite) and illite are only oversaturated within the Aldan and Lena Rivers (Supplementary Fig. 4). These waters were filtered using a 0.22 µm cutoff, and so the oversaturation of amorphous Fe, Al and Mn oxides might reflect colloidal particles that have passed through the filter. These results are consistent with mineralogical assemblages determined by transmission electron microscopy (TEM) and synchrotron-based scanning transmission X-ray microscopy (STXM) identification of colloidal and suspended particulates for the same samples, which show abundant amorphous Fe(III) ferrihydrite on the sample filters (Hirst et al., 2017), and lesser crystalline goethite and hematite, along with clay minerals. There may also be secondary minerals, such as clays, that are inherited from weathering within the soil profile (Dellinger et al., 2014).

Links between Li isotope fractionation and specific secondary mineral saturation indices have been reported in basaltic terrains (Pogge von Strandmann et al., 2006, 2010), and in glacial rivers draining permafrost in west Greenland (Wimpenny et al., 2010b). In the present study, however, there is no correlation between dissolved δ^7Li and any PHREEQC calculated mineral saturation states (Supplementary Fig 3.). This is not unexpected for rivers draining large, multi-lithology catchments, where secondary mineralogy will also vary. Whilst an abundance of amorphous and crystalline Fe oxides were observed in the secondary mineral phases on the filters for the samples in this study (Hirst et al., 2017), the presence of other secondary minerals

(particularly clay minerals) are also likely to have contributed to the δ^7Li_{susp} due to the incorporation or sorption of ^6Li.

5.3 *Topographical and catchment area controls on Li isotope fractionation*

Topography and relief can exert a strong influence on weathering. In regions unaffected by permafrost, topographically high regions are typically dominated by relatively high physical erosion with high denudation rates (often related to high uplift rates), and so high rates of exposure of fresh mineral surfaces and minimal water-rock interaction times (e.g., Montgomery and Brandon, 2002). This promotes the weathering of primary rock material and limits secondary mineral precipitation (low weathering intensity), and is expected to result in δ^7Li compositions that approach those of the primary weathering rocks. In contrast, non-permafrost rivers in low-lying regions are expected to have higher δ^7Li values, where greater water-rock interaction times promote the formation of secondary minerals and greater adsorption of Li, driving the riverine δ^7Li towards higher values. This relationship has been suggested from a broad negative correlation between δ^7Li and uplift rate in rivers from New Zealand (Pogge von Strandmann and Henderson, 2015) and in rivers draining higher elevations in the Ganges (Pogge von Strandmann et al., 2017) and the Amazon (Dellinger et al., 2015). This is also supported by generally low δ^7Li observed in rivers in the High Himalayas (Huh et al., 1998a; Kısakűrek et al., 2005).

In order to assess the effect of topography, the mean gradient of the watershed can be used as a general measure of the overall relief. At low slope angles (<15°), a broad positive linear correlation has been shown between catchment slope angle and long-term erosion rate (Montgomery and Brandon, 2002). For catchments in the CSP, LAIRA and the VMR, the mean watershed gradient was calculated using a GIS-based approach as outlined in Kutscher et al. (2017), dividing the watershed length by its maximum elevation. While a meaningful watershed gradient cannot be estimated for the overall Lena, Aldan and Viliui River catchments, a watershed gradient has been estimated for the upper catchment regions draining in to the Vilʟiui River (LR2013-62; 0.96°) and Aldan River (LR2012-13; 3.44°). Catchments of the low-lying CSP have catchment slope angles ranging from 0.24 to 1.04°. The LAIRA has catchment slope angles ranging from 0.43 to 1.65°, and rivers draining the VMR range from 0.94 to 6.34°. Both [Li] and δ^7Li_{diss} show little relationship with mean watershed gradient (Fig. 3). Despite the *ca.* five degree difference in slope angles between rivers draining the low-lying LAIRA and CSP, and the VMR, there is no clear distinction between rivers draining the mountainous and the low-lying regions, with the entire range of [Li] and

439 δ^7Li_{diss} values spanning the full range of catchment slope angles. In fact, the highest δ^7Li_{diss} values
440 observed in the Lena River watershed are from tributaries with the greatest slope angles draining
441 the Verkhoyansk Mountain Ranges.

442 The lack of a trend between δ^7Li and relief in the Lena River catchment may be due to
443 cryogenic weathering processes prevalent in regions of continuous permafrost e.g., the continual
444 supply of fresh primary minerals due to seasonal freeze-thaw cycles, frost shattering and salt
445 weathering (Woo, 2012), none of which are directly related to relief . The high degree of physical
446 erosion in permafrost-dominated catchments is widespread, and not predominantly in regions of
447 high topography as with rivers draining non-permafrost terrains (Goodfellow and Boelhouwers,
448 2013). Weathering rates can also be enhanced over predicted 'inorganic' weathering rates by
449 organic acid weathering (Huh, 2003), and could also be a factor here.

450 The [Li] and δ^7Li data are plotted against catchment area in Fig. 3. In general, discharge is
451 expected to scale with increasing catchment area (Burgers et al., 2014). Whilst no trends can be
452 seen between [Li] and catchment area (except in south-facing VMR rivers, as discussed below), a
453 broad negative trend can be seen with Li isotope composition, with greater variability observed in
454 smaller catchments, and isotopic compositions that approach the global mean value of ~23‰ with
455 larger catchment areas. This pattern likely reflects the dominance of local processes in smaller
456 catchments, which are homogenised and integrated in rivers draining larger catchments.
457
458 **5.4** *Permafrost and climatic controls on Li isotope variations*

459 Since the Lena River watershed covers a vast area, the effects of climate on the distribution
460 of Li isotopes can be considered. For this study, samples have been collected from a latitudinal and
461 climate gradient from 60° to 68° N, corresponding to mean annual air temperatures (MAAT) of −6
462 to −15°C (Gordeev and Sidorov, 1993). This corresponds to a range of maximum active layer
463 temperatures, and so reaction rates for both dissolution and secondary mineral formation, as well
464 as of depths and lengths of time of active layer thawing. To test the effects of temperature, and
465 hence climate, [Li] and δ^7Li_{diss} are shown plotted against latitude, used as a proxy for MAAT
466 (Supplementary Fig. 5). The Lena River main channel δ^7Li_{diss} values show a weak 5‰ increase from
467 the upper to the lower reaches ($R^2 = 0.47$) along the climate gradient. This progressive downstream
468 increase in δ^7Li_{diss} values observed in the Lena River main channel (Fig. 4a) is also observed in the
469 Ganges (Bagard et al., 2015) and the Changjiang Rivers (Wang et al., 2015). After the confluence of
470 the Viliui River, both Li concentrations and δ^7Li_{diss} in the Lena River main channel increase (Fig. 4).

This is unlikely to be simple mixing between the two rivers, because there are no trends between δ^7Li_{diss} and 1/[Li] (Fig. 2). Equally, anthropogenic influences from cities such as Yakutsk and Zhigansk do not appear to influence [Li] or δ^7Li_{diss}. Thus, the evolution of the Lena River δ^7Li_{diss} value likely reflects Li isotope fractionation due to precipitation or interaction with secondary minerals within the river bedload or inputs from deep groundwater into the Lena River.

Overall, there are also no clear trends in [Li] and δ^7Li_{diss} values over a *ca.* nine degree latitude gradient, suggesting that variations in the MAAT, and thus climatic conditions, do not have a dominant influence on variations in δ^7Li in the Lena River catchment. This is consistent with the results for rivers in Iceland (Pogge von Strandmann et al., 2010), rivers from different climatic zones of the Cascade Mountains (Colombia River Basalts; Liu et al., 2015) and the Mackenzie River basin (Millot et al., 2010). Interestingly, the greatest variation in both [Li] and δ^7Li_{diss} are observed in the south-facing slopes draining the VMR. South-facing slopes in permafrost regions are typically characterised by increased summer insolation and higher daily temperatures which contribute to more rapid thawing of snow cover, warmer soils, greater active layer depth and hence greater infiltration of melt water (Woo, 2012; Hindshaw et al., 2018). Repeated freezing and thawing due to earlier snow melt can destabilise the soil cover, such that south-facing slopes are typically prone to greater hillslope instability (Vasiliev, 2009; Goodfellow and Boelhouwers, 2013). This may contribute towards local variations in water flow and hence different water-rock interaction times. The lower δ^7Li_{diss} values observed in the VMR therefore likely reflect catchments dominated by lower intensity of weathering, enhanced dissolution of freshly exposed primary rock due to freeze-thaw processes and little fractionation of Li isotopes dues to reduced secondary mineral precipitation or interaction with secondary minerals within the seasonally thawed active layer (i.e., a weathering-limited regime). In contrast, the much higher δ^7Li_{diss} values might reflect increased adsorption on secondary minerals, or dissolution/reprecipitation cycles due to repeated freeze-thaw cycles that promote greater water-rock interaction, significant secondary mineral formation and therefore greater Li isotope fractionation (i.e., high weathering intensity in a transport-limited regime). However, without detailed knowledge of the thermal regime in the individual catchments, it is difficult to speculate further on these processes. A detailed study of the cryogenic weathering processes occurring within a small, well-constrained river catchment draining continuous permafrost would shed some light on the relative importance of these contrasting processes.

5.5 *Modelled Rayleigh fractionation factors and water residence time - Li/Na*

Li and Na are both monovalent alkali metals that reside in primary silicate minerals, and are readily mobilised into solution during weathering processes. During weathering, it is assumed that Li and Na are released congruently, and the Li/Na ratio is progressively diminished by the incremental removal of Li through interaction with secondary minerals that preferentially remove ^{6}Li, either by adsorption onto the surface, by trapping within the interlayer (in the case of 2:1 clays), or by incorporation into the mineral structure. This in turn increases $\delta^{7}Li$ values and decreases Li/Na values in waters. Values for $\delta^{7}Li_{diss}$ are plotted against Li/Na ratios in Figure 5, where a broad negative correlation between these two parameters is evident and similar to that observed in other river systems (Millot et al., 2010; Bagard et al., 2015; Liu et al., 2015; Wang et al., 2015).

The relationship between Li removal into secondary minerals and associated Li isotope fractionation was investigated using a modelling approach found in other studies (Pogge von Strandmann et al., 2010b; Bouchez et al., 2013; Dellinger et al., 2014; Bagard et al., 2015; Pogge von Strandmann et al., 2017). The model considers water within a watershed (i.e. groundwaters and surface waters) that initially has Li/Na and $\delta^{7}Li$ values equal to those of weathering rocks. It is assumed that Li and Na are released together and that Li isotopes are not fractionated by dissolution processes. Lithium then is only progressively depleted in the water by incremental loss of Li (while the Li remaining in the water is well-mixed). This loss results in fractionation of Li isotopes, since Li adsorbed on, or incorporated into, secondary minerals has a lower $^{7}Li/^{6}Li$ than that of Li in the water. In this case, the value of $\delta^{7}Li$ of Li in the water will increase as Li/Na decreases according to a Rayleigh distillation relationship that is controlled by the fractionation factor (α) that reflects the preferential removal of ^{6}Li.

$$\delta^{7}Li_{diss} = \delta^{7}Li_{0} + 1000(\alpha-1)\ln(f_{\mathrm{diss}}^{\mathrm{Li}}) \qquad (1)$$

where $\delta^{7}Li_{diss}$ is the Li isotope composition of the dissolved phase and $\delta^{7}Li_{0}$ is the value for Li released into the water, equal to the mean $\delta^{7}Li_{rock}$ of the weathered rocks. The term $f_{\mathrm{diss}}^{\mathrm{Li}}$ is the fraction of Li remaining in solution, calculated using the equation:

$$f_{\mathrm{diss}}^{\mathrm{Li}} = \frac{\mathrm{Li/Na_{diss}}}{\mathrm{Li/Na_{0}}} \qquad (2)$$

The fractionation lines represent the calculated compositions of waters subjected to different degrees of Li removal from a single starting Li/Na and δ^7Li composition. A starting isotopic composition (δ^7Li_0) of 0‰ is used, which is a representative value for the average upper continental crust. Changing δ^7Li_0 to values of -2 to +5‰ observed in riverine suspended sediments, shales and upper continental crustal rocks and basalts will result in small shifts in the model curves (not shown), although this will not substantially affect the range of fractionation factors needed to explain the range of measured compositions. The bedrock Li/Na ratio (and hence the initial ratio of Li/Na released into waters), is difficult to constrain for such a large, multi-lithological catchment and undoubtedly varies between sub-catchments and across the watershed. To account for a range of possible end-member values, a Li/Na_0 molar ratio of 0.03, equal to the highest dissolved value found in the Lena catchment area, and a value of 0.1, which is that of the upper continental crust (Taylor and McLennan, 1995) have been adopted in the model calculations. This range of initial Li/Na_0 are depicted by the grey box in Fig. 5.

The range of data within the Lena River catchment cannot be explained by a single isotopic fractionation factor. The majority of data fall within the curves for α values ranging from ~0.997 to 0.990 (Δ^7Li = -3‰ and -10‰). However, a number of outliers (particularly for rivers draining south-facing slopes within the VMR) fall outside these α values, requiring a wider range of fractionation factors. The range of isotopic fractionation factors in Fig. 5 are consistent with experimentally determined values for various secondary minerals, including those predicted to be oversaturated within the Lena River (see section 5.2), with $\alpha_{vermiculite}$ = 0.971, $\alpha_{kaolinite}$ = 0.979, $\alpha_{gibbsite}$ = 0.984-0.993, $\alpha_{ferrihydrite}$ ≈ 0.998, and $\alpha_{smectite}$ = 0.984 (Zhang et al. 1998; Pistiner and Henderson, 2003; Millot and Girard, 2007; Vigier et al. 2008; Wimpenny et al. 2015). The range of α is also comparable to that those observed in other global rivers (e.g., Amazon (Dellinger et al., 2015); Ganges (Bagard et al., 2015; Pogge von Strandmann et al., 2017)). Overall, the range of fractionation factors required to explain the data reflects the complex behavior of Li in such a vast catchment. Other processes such as adsorption, precipitation in other phases, or interaction with organics, may also result in a wider variation in fractionation factors. It is likely that there are also other processes within each watershed that have caused variations in the relationship between Li/Na and δ^7Li values. For example, mixing occurs amongst different sub-surface and surface waters with different evolutionary histories and so different Li characteristics. In addition, variability may be caused by the uptake of Na into some secondary minerals (such as clays or zeolites), and/or desorption of Na

564 from mineral surfaces in soils, thus decoupling Li/Na from δ^7Li. It is not possible to distinguish
565 whether these processes occur within the river, or is controlled by sub-surface residence time.
566
567 **5.6** *Comparison with global rivers*
568 Huh et al. (1998a) also measured dissolved δ^7Li in the Lena River catchment, and several other
569 Siberian rivers. They observed a wide range in δ^7Li values (~6 to 30‰), similar to the values
570 observed in this study. The dissolved δ^7Li observed in the Lena River catchment (from this study
571 and Huh et al. 1998a) overlap with those of other polar, cold climate rivers that are underlain by
572 continuous, discontinuous, sporadic or isolated permafrost (e.g., the Mackenzie River basin (~9 to
573 29‰; Millot et al. 2010)), Svalbard (~8 to 14‰; Hindshaw et al. (2018)) and Antarctic rivers (~12 to
574 23‰; Witherow et al. (2010)). They also overlap with values from glaciated and non-glaciated rivers
575 in west Greenland that are underlain by permafrost (~14 to 36‰; Wimpenny et al. (2010b), and
576 those of rivers in Iceland that are unaffected by permafrost (Pogge von Strandmann et al. (2006);
577 Vigier et al. (2009).
578 Interestingly, the overall range in δ^7Li and Li/Na values in these cold climate, polar regions
579 (including regions impacted by permafrost and glacial weathering processes) are similar to those
580 found in temperate and tropical rivers (Fig. 6). It has been proposed that weathering rates are
581 strongly controlled by temperature and hence climate (precipitation and runoff) (e.g. West et al.,
582 2005; Gislason et al., 2009). Warmer, wetter watersheds are expected to have greater chemical
583 weathering rates than watersheds in high latitude permafrost-dominated regions, where the cold
584 climate and restricted water-rock and water-soil interactions are predicted to reduce the rate of
585 chemical weathering (Huh and Edmond, 1999). Whilst Li isotopes cannot constrain the rates of
586 silicate weathering (for a discussion, see Pogge von Strandmann et al., 2017), the magnitude of Li
587 isotope fractionation, and hence intensity of weathering (i.e., the rate of secondary mineral
588 formation relative to the rate of primary mineral dissolution) observed in such cold climate, polar
589 regions is partly due to the increased availability of Li in primary minerals due to enhanced physical
590 erosion facilitating greater chemical weathering. The unique role of cryogenic weathering
591 processes such as repeat freeze-thaw cycles, frost shattering and salt weathering continually
592 expose fresh primary minerals and prevents the accumulation of weathered products and
593 development of thick soil profiles. The high degree of physical erosion, together with chemical
594 weathering in the presence of organic acids is sufficient to overcome the temperature inhibition on
595 the mineral reaction kinetics (Huh et al., 1998c; Huh et al., 1998b; Huh and Edmond, 1999).

Global rivers are further compared in Figure 7, which shows the frequency of dissolved Li isotope data for some of the large global rivers and rivers draining basaltic terrains. Typically, the Ganges, Lena and basalts all have similar frequency peaks, clustering around the global riverine mean of ~23‰ (Huh et al., 1998a). Rivers draining the high Himalayas have a slightly lower average value (~14 to 16‰), consistent with greater exposure rates of fresh rock driving the Li isotopic compositions towards crustal rock values. Interestingly, the Amazon and Mackenzie Rivers have the lightest mean values of these large datasets, of ~16‰. Hence, the mean values of these different catchments are quite similar relative to the overall variability in δ^7Li observed in rivers. This, in combination with the trends with Li/Na, further supports the conclusion that climatic controls (e.g., temperature and runoff) are weak secondary controls on Li isotopes and hence silicate weathering processes of primary rock dissolution relative to secondary mineral formation. The data therefore suggest that similar processes control global Li geochemistry in rivers from cold, temperate and tropical regions.

This has implications for the use of δ^7Li as a palaeo-weathering tracer, because it implies that the global riverine mean of 23‰ is not the result of mixing Li with a wide range of δ^7Li values in different rivers (as it is, for example, for $^{87}Sr/^{86}Sr$; Palmer and Edmond, 1989), but rather that many major rivers share a value of ~23‰, irrespective of climate and weathering regime. This therefore suggests that in order to explain the $\delta^7Li_{seawater}$ ~9‰ increase observed during the early Cenozoic (Hathorne and James, 2006; (Misra and Froelich, 2012)), the global weathering conditions would have to have significantly changed from low weathering intensity conditions imparting low riverine δ^7Li_{diss} input to the oceans, to the present day weathering conditions imparting a mean riverine δ^7Li_{diss} of 23‰. Hence, if the global riverine δ^7Li is not principally controlled by climate, this may suggest that the Cenozoic Li curve may be more significantly controlled by changing riverine fluxes (Wanner et al., 2014), rather than isotope ratios, possibly coupled with changes associated with the removal of Li from the oceans (Li and West, 2014; Coogan et al., 2017).

6. Conclusions

In this study, we report Li data for over 70 river waters and 11 suspended sediments from the Lena River Basin, a large, complex, multi-lithological catchment underlain by continuous permafrost discharging into the Arctic Ocean. A fractionation factor (α) during weathering of between ~ 0.997 and 0.990 can explain the data for the Lena River, comparable to previously published experimental and field based values from highly disparate climates and weathering regimes. Contrary to reports

628 from other studies from rivers in non-permafrost terrains, there are no systematic trends observed
629 between riverine δ^7L_{diss} and watershed mean slope angle (a proxy for erosion rate), and so between
630 values for rivers draining the Verkhyansk Mountain Range (VMR) when compared to those for low-
631 lying rivers of the Central Siberian Plateau. South-facing catchments from the VMR exhibit more
632 δ^7Li variation than other areas, likely due to the higher insolation affecting the thickness of the
633 active layer. Cryogenic weathering processes found in permafrost-dominated regions may obscure
634 any topographical controls on Li isotope fractionation observed in rivers draining non-permafrost.
635 At the basin scale, the Lena River has a remarkably similar range in δ^7Li values to global rivers
636 from contrasting climate and weathering regimes from polar, temperate and tropical regions.
637 Overall, temperature, the presence of permafrost, and indeed climate are weak controls on riverine
638 Li isotope compositions, and similar processes (that is, the balance between primary silicate mineral
639 dissolution and the preferential incorporation or adsorption of ^{6}Li during formation of secondary
640 minerals) that operate in different climates control global riverine Li geochemistry. This suggests
641 that climate changes likely will little affect the isotope composition of Li delivered to the ocean, and
642 changing riverine flux must be considered when using sedimentary records of Li isotopes to
643 understand changes in past weathering regimes.
644
645 **Acknowledgements**
646 This project was funded by the Swedish Research Council (VR 621-2010-3917), the Swedish Polar
647 Research Secretariat (SIMO 2011-165 and 2012-213) and MetTrans, an EU FP7 Marie Curie Initial
648 Training Network grant. We would like to thank Phil Holdship for his assistance with trace element
649 analysis, Yu-Te (Alan) Hsieh for help with the MC-ICP-MS and Jon Wade for assistance with data
650 presentation. We also thank Fang-Zhen Teng (Associate Editor), Josh Wimpenny, and two
651 anonymous reviewers for constructive comments on an earlier version of the manuscript. PPvS and
652 MJM are supported by ERC Consolidator grant 682760 - CONTROLPASTCO2.
653
654 **References**
655
656 Bagard M.-L., West A. J., Newman K. and Basu A. R. (2015) Lithium isotope fractionation in the
657 Ganges–Brahmaputra floodplain and implications for groundwater impact on seawater
658 isotopic composition. *Earth Planet. Sci. Lett.* **432**, 404–414. Available at:
659 http://www.sciencedirect.com/science/article/pii/S0012821X15005622 [Accessed November
660 29, 2015].

661 Berner R. A., Lasaga A. C. and Garrels R. M. (1983) The carbonate-silicate geochemical cycle and its
662 effect on atmospheric carbon dioxide over the past 100 million years. *Am. J. Sci.* **283**, 641–
663 683.
664 Bouchez J., von Blanckenburg F. and Schuessler J. A. (2013) Modeling novel stable isotope ratios in
665 the weathering zone. *Am. J. Sci.* **313**, 267–308. Available at:
666 http://www.ajsonline.org/content/313/4/267.abstract.
667 Brown J., Ferrians Jr. O. J., Heginbottom J. A. and Melnikov E. S. (1997) *Circum-Arctic map of*
668 *permafrost and ground-ice conditions*., Available at:
669 http://pubs.er.usgs.gov/publication/cp45.
670 Burgers H. E. (Robin), Schipper A. M. and Jan Hendriks A. (2014) Size relationships of water
671 discharge in rivers: scaling of discharge with catchment area, main-stem length and
672 precipitation. *Hydrol. Process.* **28**, 5769–5775. Available at:
673 http://dx.doi.org/10.1002/hyp.10087.
674 Chan L. H., Edmond J. M., Thompson G. and Gillis K. (1992) Lithium isotopic composition of
675 submarine basalts: implications for the lithium cycle in the oceans. *Earth Planet. Sci. Lett.* **108**,
676 151–160.
677 Chevychelov A. P. and Bosikov N. P. (2010) Natural Conditions BT - The Far North: Plant
678 Biodiversity and Ecology of Yakutia. In (eds. E. I. Troeva, A. P. Isaev, M. M. Cherosov, and N. S.
679 Karpov). Springer Netherlands, Dordrecht. pp. 1–23. Available at:
680 https://doi.org/10.1007/978-90-481-3774-9_1.
681 Coogan L. A., Gillis K. M., Pope M. and Spence J. (2017) The role of low-temperature (off-axis)
682 alteration of the oceanic crust in the global Li-cycle: Insights from the Troodos ophiolite.
683 *Geochim. Cosmochim. Acta* **203**, 201–215. Available at:
684 http://www.sciencedirect.com/science/article/pii/S0016703717300066 [Accessed June 12,
685 2017].
686 Dellinger M., Gaillardet J., Bouchez J., Calmels D., Galy V., Hilton R. G., Louvat P. and France-Lanord
687 C. (2014) Lithium isotopes in large rivers reveal the cannibalistic nature of modern
688 continental weathering and erosion. *Earth Planet. Sci. Lett.* **401**, 359–372. Available at:
689 http://www.sciencedirect.com/science/article/pii/S0012821X14003793 [Accessed March 30,
690 2016].
691 Dellinger M., Gaillardet J., Bouchez J., Calmels D., Louvat P., Dosseto A., Gorge C., Alanoca L. and
692 Maurice L. (2015) Riverine Li isotope fractionation in the Amazon River basin controlled by
693 the weathering regimes. *Geochim. Cosmochim. Acta* **164**, 71–93. Available at:
694 http://www.sciencedirect.com/science/article/pii/S0016703715002483.
695 Eiriksdottir E. S., Gislason S. R. and Oelkers E. H. (2013) Does temperature or runoff control the
696 feedback between chemical denudation and climate? Insights from NE Iceland. *Geochim.*
697 *Cosmochim. Acta* **107**, 65–81.
698 Elliott T., Thomas A., Jeffcoate A. and Niu Y. (2006) Lithium isotope evidence for subduction-
699 enriched mantle in the source of mid-ocean-ridge basalts. *Nature* **443**, 565–568. Available at:
700 http://dx.doi.org/10.1038/nature05144.
701 Fedorov A. N., Ivanova R. N., Park H., Hiyama T. and Iijima Y. (2014) Recent air temperature
702 changes in the permafrost landscapes of northeastern Eurasia. *Polar Sci.* **8**, 114–128.
703 Available at: http://www.sciencedirect.com/science/article/pii/S187396521400019X
704 [Accessed March 26, 2016].
705 Flesch G. D., Anderson A. R. and Svec H. J. (1973) A secondary isotopic standard for 6Li/7Li
706 determinations. *Int. J. Mass Spectrom. Ion Phys.* **12**, 265–272. Available at:
707 http://www.sciencedirect.com/science/article/pii/0020738173800439 [Accessed January 5,

2016].
Frey K. E. and McClelland J. W. (2009) Impacts of permafrost degradation on arctic river biogeochemistry. *Hydrol. Process.* **23**, 169–182. Available at: http://dx.doi.org/10.1002/hyp.7196.
Frings P. J., Clymans W., Fontorbe G., Gray W., Chakrapani G. J., Conley D. J. and De La Rocha C. (2015) Silicate weathering in the Ganges alluvial plain. *Earth Planet. Sci. Lett.* **427**, 136–148. Available at: http://linkinghub.elsevier.com/retrieve/pii/S0012821X15004124 [Accessed March 12, 2017].
Gislason S. R., Arnorsson S. and Armannsson H. (1996) Chemical weathering of basalt in Southwest Iceland; effects of runoff, age of rocks and vegetative/glacial cover. *Am. J. Sci.* **296**, 837–907. Available at: http://www.ajsonline.org/content/296/8/837.short.
Goodfellow B. W. and Boelhouwers J. (2013) 7.31 Hillslope Processes in Cold Environments: An Illustration of High-Latitude Mountain and Hillslope Processes and Forms. In *Treatise on Geomorphology* (ed. J. F. Shroder). Academic Press, San Diego. pp. 320–336. Available at: http://www.sciencedirect.com/science/article/pii/B9780123747396001810.
Gordeev V. V, Martin J. M., Sidorov I. S. and Sidorova M. V (1996) A reassessment of the Eurasian river input of water, sediment, major elements, and nutrients to the Arctic Ocean. *Am. J. Sci.* **296**, 664–691. Available at: http://www.ajsonline.org/content/296/6/664.short.
Gordeev V. V and Sidorov I. S. (1993) Concentrations of major elements and their outflow into the Laptev Sea by the Lena River. *Mar. Chem.* **43**, 33–45. Available at: http://www.sciencedirect.com/science/article/pii/0304420393902149.
Hathorne E. C. and James R. H. (2006) Temporal record of lithium in seawater: A tracer for silicate weathering? *Earth Planet. Sci. Lett.* **246**, 393–406. Available at: http://www.sciencedirect.com/science/article/pii/S0012821X06003086.
Henchiri S., Gaillardet J., Dellinger M., Bouchez J. and Spencer R. G. M. (2016) Temporal variations of riverine dissolved lithium isotopic signatures unveil contrasting weathering regimes in low-relief Central Africa. *Geophys. Res. Lett.*, n/a-n/a. Available at: http://doi.wiley.com/10.1002/2016GL067711 [Accessed March 30, 2016].
Hilley G. E., Chamberlain C. P., Moon S., Porder S. and Willett S. D. (2010) *Competition between erosion and reaction kinetics in controlling silicate-weathering rates*.,
Hindshaw R. S., Aciego S. M. and Tipper E. T. (2018) Li and U Isotopes as a Potential Tool for Monitoring Active Layer Deepening in Permafrost Dominated Catchments. *Front. Earth Sci.* **6**, 102. Available at: https://www.frontiersin.org/article/10.3389/feart.2018.00102.
Hindshaw R. S., Heaton T. H. E., Boyd E. S., Lindsay M. R. and Tipper E. T. (2016) Influence of glaciation on mechanisms of mineral weathering in two high Arctic catchments. *Chem. Geol.* **420**, 37–50.
Hirst C., Andersson P. S., Shaw S., Burke I. T., Kutscher L., Murphy M. J., Maximov T., Pokrovsky O. S., Mörth C.-M. and Porcelli D. (2017) Characterisation of Fe-bearing particles and colloids in the Lena River basin, NE Russia. *Geochim. Cosmochim. Acta* **213**, 553–573. Available at: https://www.sciencedirect.com/science/article/pii/S0016703717304209 [Accessed March 10, 2018].
Holmes R. M., McClelland J. W., Tank S. E., Spencer R. G. M. and Shiklomanov A. I. (2018) Arctic Great Rivers Observatory. Water Quality Dataset Version 20180321. Available at: https://www.arcticgreatrivers.org/data.
Huh Y. (2003) Chemical weathering and climate --- a global experiment: A review. *Geosci. J.* **7**, 277–288. Available at: http://dx.doi.org/10.1007/BF02910294.
Huh Y., Chan L.-H. and Edmond J. M. (2001) Lithium isotopes as a probe of weathering processes:

Orinoco River. *Earth Planet. Sci. Lett.* **194**, 189–199. Available at: http://www.sciencedirect.com/science/article/pii/S0012821X01005234.

Huh Y., Chan L.-H., Zhang L. and Edmond J. M. (1998a) Lithium and its isotopes in major world rivers: implications for weathering and the oceanic budget. *Geochim. Cosmochim. Acta* **62**, 2039–2051. Available at: http://www.sciencedirect.com/science/article/pii/S0016703798001264 [Accessed April 7, 2017].

Huh Y. and Edmond J. M. (1999) The fluvial geochemistry of the rivers of Eastern Siberia: III. Tributaries of the Lena and Anabar draining the basement terrain of the Siberian Craton and the Trans-Baikal Highlands. *Geochim. Cosmochim. Acta* **63**, 967–987. Available at: http://www.sciencedirect.com/science/article/pii/S0016703799000459 [Accessed March 25, 2016].

Huh Y., Panteleyev G., Babich D., Zaitsev A. and Edmond J. M. (1998b) The fluvial geochemistry of the rivers of Eastern Siberia: II. Tributaries of the Lena, Omoloy, Yana, Indigirka, Kolyma, and Anadyr draining the collisional/accretionary zone of the Verkhoyansk and Cherskiy ranges. *Geochim. Cosmochim. Acta* **62**, 2053–2075. Available at: http://www.sciencedirect.com/science/article/pii/S0016703798001276 [Accessed February 25, 2016].

Huh Y., Tsoi M.-Y., Zaitsev A. and Edmond J. M. (1998c) The fluvial geochemistry of the rivers of Eastern Siberia: I. tributaries of the Lena River draining the sedimentary platform of the Siberian Craton. *Geochim. Cosmochim. Acta* **62**, 1657–1676. Available at: http://www.sciencedirect.com/science/article/pii/S0016703798001070 [Accessed February 25, 2016].

Kısakűrek B., James R. H. and Harris N. B. W. (2005) Li and δ7Li in Himalayan rivers: Proxies for silicate weathering? *Earth Planet. Sci. Lett.* **237**, 387–401. Available at: http://www.sciencedirect.com/science/article/pii/S0012821X05005005.

Kutscher L., Mörth C.-M., Porcelli D., Hirst C., Maximov T. C., Petrov R. E. and Andersson P. S. (2017) Spatial variation in concentration and sources of organic carbon in the Lena River, Siberia. *J. Geophys. Res. Biogeosciences* **122**, 1999–2016. Available at: http://dx.doi.org/10.1002/2017JG003858.

Lemarchand E., Schott J. and Gaillardet J. (2007) How surface complexes impact boron isotope fractionation: Evidence from Fe and Mn oxides sorption experiments. *Earth Planet. Sci. Lett.* **260**, 277–296. Available at: http://www.sciencedirect.com/science/article/pii/S0012821X07003469.

Li G. and West A. J. (2014) Evolution of Cenozoic seawater lithium isotopes: Coupling of global denudation regime and shifting seawater sinks. *Earth Planet. Sci. Lett.* **401**, 284–293. Available at: http://www.sciencedirect.com/science/article/pii/S0012821X14003884.

Liu C.-Q., Zhao Z.-Q., Wang Q. and Gao B. (2011) Isotope compositions of dissolved lithium in the rivers Jinshajiang, Lancangjiang, and Nujiang: Implications for weathering in Qinghai-Tibet Plateau. *Appl. Geochemistry* **26**, **Supple**, S357–S359. Available at: http://www.sciencedirect.com/science/article/pii/S0883292711001387.

Liu X.-M., Wanner C., Rudnick R. L. and McDonough W. F. (2015) Processes controlling δ7Li in rivers illuminated by study of streams and groundwaters draining basalts. *Earth Planet. Sci. Lett.* **409**, 212–224. Available at: http://www.sciencedirect.com/science/article/pii/S0012821X14006591.

Manaka T., Araoka D., Yoshimura T., Hossain H. M. Z., Nishio Y., Suzuki A. and Kawahata H. (2017) Downstream and seasonal changes of lithium isotope ratios in the Ganges-Brahmaputra river

system. *Geochemistry, Geophys. Geosystems* **18**, 3003–3015. Available at: http://dx.doi.org/10.1002/2016GC006738.
Millot R., Gaillardet J. érôme, Dupré B. and Allègre C. J. (2003) Northern latitude chemical weathering rates: clues from the Mackenzie River Basin, Canada. *Geochim. Cosmochim. Acta* **67**, 1305–1329. Available at: http://www.sciencedirect.com/science/article/pii/S0016703702012073.
Millot R. and Girard J. P. (2007) Lithium Isotope Fractionation during adsorption onto mineral surfaces. In *Clays in natural & engineered barriers for radioactive waste confinement. 3rd International meeting* Lille, France.
Millot R., Vigier N. and Gaillardet J. (2010) Behaviour of lithium and its isotopes during weathering in the Mackenzie Basin, Canada. *Geochim. Cosmochim. Acta* **74**, 3897–3912. Available at: http://www.sciencedirect.com/science/article/pii/S0016703710002103.
Misra S. and Froelich P. N. (2012) Lithium Isotope History of Cenozoic Seawater: Changes in Silicate Weathering and Reverse Weathering. *Science (80-.).* **335**, 818–823. Available at: http://www.sciencemag.org/content/335/6070/818.abstract.
Montgomery D. R. and Brandon M. T. (2002) Topographic controls on erosion rates in tectonically active mountain ranges. *Earth Planet. Sci. Lett.* **201**, 481–489. Available at: http://www.sciencedirect.com/science/article/pii/S0012821X02007252.
Nezat C. A., Lyons W. B. and Welch K. A. (2001) Chemical weathering in streams of a polar desert (Taylor Valley, Antarctica). *Geol. Soc. Am. Bull.* **113**, 1401–1408. Available at: http://gsabulletin.gsapubs.org/content/113/11/1401.abstract.
Palmer M. R. and Edmond J. M. (1989) The strontium isotope budget of the modern ocean. *Earth Planet. Sci. Lett.* **92**, 11–26. Available at: http://www.sciencedirect.com/science/article/pii/0012821X89900174.
Parkhurst D. L. and Appelo C. A. J. (1999) *User's guide to PHREEQC (Version 2): a computer program for speciation, batch-reaction, one-dimensional transport, and inverse geochemical calculations*.,
Pistiner J. S. and Henderson G. M. (2003) Lithium-isotope fractionation during continental weathering processes. *Earth Planet. Sci. Lett.* **214**, 327–339. Available at: http://www.sciencedirect.com/science/article/pii/S0012821X03003480.
Pogge von Strandmann P. A. E., Burton K. W., James R. H., van Calsteren P. and Gislason, S. R. (2010a) Assessing the role of climate on uranium and lithium isotope behaviour in rivers draining a basaltic terrain. *Chem. Geol.* **270**, 227–239.
Pogge von Strandmann P. A. E., Burton K. W., James R. H., van Calsteren P., Gíslason S. R. and Mokadem F. (2006) Riverine behaviour of uranium and lithium isotopes in an actively glaciated basaltic terrain. *Earth Planet. Sci. Lett.* **251**, 134–147. Available at: http://www.sciencedirect.com/science/article/pii/S0012821X06006388 [Accessed April 4, 2016].
Pogge von Strandmann P. A. E., Burton K. W., Opfergelt S., Eiríksdóttir E. S., Murphy M. J., Einarsson A. and Gislason S. R. (2016) The effect of hydrothermal spring weathering processes and primary productivity on lithium isotopes: Lake Myvatn, Iceland. *Chem. Geol.* Available at: http://linkinghub.elsevier.com/retrieve/pii/S0009254116301000 [Accessed March 8, 2016].
Pogge von Strandmann P. A. E., Elliott T., Marschall H. R., Coath C., Lai Y.-J., Jeffcoate A. B. and Ionov D. A. (2011) Variations of Li and Mg isotope ratios in bulk chondrites and mantle xenoliths. *Geochim. Cosmochim. Acta* **75**, 5247–5268. Available at: http://www.sciencedirect.com/science/article/pii/S0016703711003644.

Pogge von Strandmann P. A. E., Frings P. J. and Murphy M. J. (2017) Lithium isotope behaviour during weathering in the Ganges Alluvial Plain. *Geochim. Cosmochim. Acta* **198**, 17–31.
Pogge von Strandmann P. A. E. and Henderson G. M. (2015) The Li isotope response to mountain uplift. *Geology* **43**, 67–70. Available at: http://geology.gsapubs.org/content/43/1/67.abstract.
Pogge von Strandmann P. A. E., James R. H., van Calsteren P. and Gislason S. R. (2010b) Assessing the role of climate on uranium and lithium isotope behaviour in rivers draining a basaltic terrain. *Chem. Geol.* **270**, 227–239. Available at: http://www.sciencedirect.com/science/article/pii/S0009254109004690.
Pogge von Strandmann P. A. E., Jenkyns H. C. and Woodfine R. G. (2013) Lithium isotope evidence for enhanced weathering during Oceanic Anoxic Event 2. *Nat. Geosci* **6**, 668–672. Available at: http://dx.doi.org/10.1038/ngeo1875.
Pokrovsky O. S., Schott J., Kudryavtzev D. I. and Dupré B. (2005) Basalt weathering in Central Siberia under permafrost conditions. *Geochim. Cosmochim. Acta* **69**, 5659–5680.
Raymo M. E. and Ruddiman W. F. (1992) Tectonic forcing of late Cenozoic climate. *Nature* **359**, 117–122. Available at: http://dx.doi.org/10.1038/359117a0.
Raymo M. E., Ruddiman W. F. and Froelich P. N. (1988) Influence of late Cenozoic mountain building on ocean geochemical cycles. *Geol.* **16**, 649–653. Available at: http://geology.gsapubs.org/content/16/7/649.abstract.
Sauzéat L., Rudnick R. L., Chauvel C., Garçon M. and Tang M. (2015) New perspectives on the Li isotopic composition of the upper continental crust and its weathering signature. *Earth Planet. Sci. Lett.* **428**, 181–192. Available at: http://www.sciencedirect.com/science/article/pii/S0012821X15004677 [Accessed March 25, 2016].
Stallard R. F. and Edmond J. M. (1983) Geochemistry of the Amazon: 2. The influence of geology and weathering environment on the dissolved load. *J. Geophys. Res. Ocean.* **88**, 9671–9688. Available at: http://doi.wiley.com/10.1029/JC088iC14p09671 [Accessed November 17, 2016].
Sun X., Mörth C.-M., Porcelli D., Kutscher L., Hirst C., Murphy M. J., Maximov T., Petrov R. E., Humborg C., Schmitt M. and Andersson P. S. (2018) Stable silicon isotopic compositions of the Lena River and its tributaries: Implications for silicon delivery to the Arctic Ocean. *Geochim. Cosmochim. Acta* **241**, 120–133. Available at: https://www.sciencedirect.com/science/article/pii/S0016703718304976?dgcid=rss_sd_all [Accessed October 14, 2018].
Sun X., Mörth C.-M., Porcelli D., Kutscher L., Hirst C., Murphy M. J., Maximov T., Petrov R. E., Humborg C., Schmitt M. and Andersson P. S. w. *Geochim. Cosmochim. Acta*.
Taylor S. R. and McLennan S. M. (1995) The geochemical evolution of the continental crust. *Rev. Geophys.* **33**, 241–265. Available at: http://dx.doi.org/10.1029/95RG00262.
Teng F.-Z., McDonough W. F., Rudnick R. L., Dalpé C., Tomascak P. B., Chappell B. W. and Gao S. (2004) Lithium isotopic composition and concentration of the upper continental crust. *Geochim. Cosmochim. Acta* **68**, 4167–4178. Available at: http://www.sciencedirect.com/science/article/pii/S0016703704004326.
Tomascak P. B., Langmuir C. H., le Roux P. J. and Shirey S. B. (2008) Lithium isotopes in global mid-ocean ridge basalts. *Geochim. Cosmochim. Acta* **72**, 1626–1637. Available at: http://www.sciencedirect.com/science/article/pii/S0016703708000185.
Vasiliev I. S. (2009) Mountain permafrost landscapes of Yakutia. *Geogr. Nat. Resour.* **30**, 92–95. Available at: http://www.sciencedirect.com/science/article/pii/S1875372809000185.
Vigier N., Decarreau A., Millot R., Carignan J., Petit S. and France-Lanord C. (2008) Quantifying Li isotope fractionation during smectite formation and implications for the Li cycle. *Geochim.*

Cosmochim. Acta **72**, 780–792. Available at: http://www.sciencedirect.com/science/article/pii/S0016703707006680.
Vigier N., Gislason S. R., Burton K. W., Millot R. and Mokadem F. (2009) The relationship between riverine lithium isotope composition and silicate weathering rates in Iceland. *Earth Planet. Sci. Lett.* **287**, 434–441. Available at: http://www.sciencedirect.com/science/article/pii/S0012821X09004993.
Vigier N. and Goddéris Y. (2015) A new approach for modeling Cenozoic oceanic lithium isotope paleo-variations: the key role of climate. *Clim. Past* **11**, 635–645. Available at: http://www.clim-past.net/11/635/2015/ [Accessed August 7, 2017].
Walker J. C. G., Hays P. B. and Kasting J. F. (1981) A negative feedback mechanism for the long-term stabilization of Earth's surface temperature. *J. Geophys. Res.* **86**, 9776. Available at: http://doi.wiley.com/10.1029/JC086iC10p09776 [Accessed September 21, 2016].
Wang Q.-L., Chetelat B., Zhao Z.-Q., Ding H., Li S.-L., Wang B.-L., Li J. and Liu X.-L. (2015) Behavior of lithium isotopes in the Changjiang River system: Sources effects and response to weathering and erosion. *Geochim. Cosmochim. Acta* **151**, 117–132. Available at: http://www.sciencedirect.com/science/article/pii/S0016703714007248.
Wanner C., Sonnenthal E. L. and Liu X. M. (2014) Seawater δ7Li: A direct proxy for global CO2 consumption by continental silicate weathering? *Chem. Geol.* **381**.
West A. J., Galy A. and Bickle M. (2005) Tectonic and climatic controls on silicate weathering. *Earth Planet. Sci. Lett.* **235**, 211–228. Available at: http://www.sciencedirect.com/science/article/pii/S0012821X05002116.
Weynell M., Wiechert U. and Schuessler J. A. (2017) Lithium isotopes and implications on chemical weathering in the catchment of Lake Donggi Cona, northeastern Tibetan Plateau. *Geochim. Cosmochim. Acta* **213**, 155–177. Available at: http://linkinghub.elsevier.com/retrieve/pii/S0016703717303757 [Accessed August 20, 2017].
Wimpenny J., Colla C. A., Yu P., Yin Q. Z., Rustad J. R. and Casey W. H. (2015) Lithium isotope fractionation during uptake by gibbsite. *Geochim. Cosmochim. Acta* **168**.
Wimpenny J., Gíslason S. R., James R. H., Gannoun A., Pogge Von Strandmann P. A. E. and Burton K. W. (2010a) The behaviour of Li and Mg isotopes during primary phase dissolution and secondary mineral formation in basalt. *Geochim. Cosmochim. Acta* **74**, 5259–5279. Available at: http://www.sciencedirect.com/science/article/pii/S0016703710003698.
Wimpenny J., James R. H., Burton K. W., Gannoun A., Mokadem F. and Gíslason S. R. (2010b) Glacial effects on weathering processes: New insights from the elemental and lithium isotopic composition of West Greenland rivers. *Earth Planet. Sci. Lett.* **290**, 427–437. Available at: http://www.sciencedirect.com/science/article/pii/S0012821X10000051.
Witherow R. A., Lyons W. B. and Henderson G. M. (2010) Lithium isotopic composition of the McMurdo Dry Valleys aquatic systems. *Chem. Geol.* **275**, 139–147.
Woo M. (2012) *Permafrost Hydrology*., Springer Berlin Heidelberg.
Ye B., Yang D. and Kane D. L. (2003) Changes in Lena River streamflow hydrology: Human impacts versus natural variations. *Water Resour. Res.* **39**. Available at: http://doi.wiley.com/10.1029/2003WR001991 [Accessed March 26, 2016].
Ye B., Yang D., Zhang Z. and Kane D. L. (2009) Variation of hydrological regime with permafrost coverage over Lena Basin in Siberia. *J. Geophys. Res. Atmos.* **114**.
Yoon J. (2010) Lithium as a Silicate Weathering Proxy: Problems and Perspectives. *Aquat. Geochemistry* **16**, 189–206. Available at: http://dx.doi.org/10.1007/s10498-009-9078-z.
Zhang L., Chan L.-H. and Gieskes J. M. (1998) Lithium isotope geochemistry of pore waters from ocean drilling program Sites 918 and 919, Irminger Basin. *Geochim. Cosmochim. Acta* **62**,

943 2437–2450. Available at:
944 http://www.sciencedirect.com/science/article/pii/S0016703798001781.
945
946

Figures

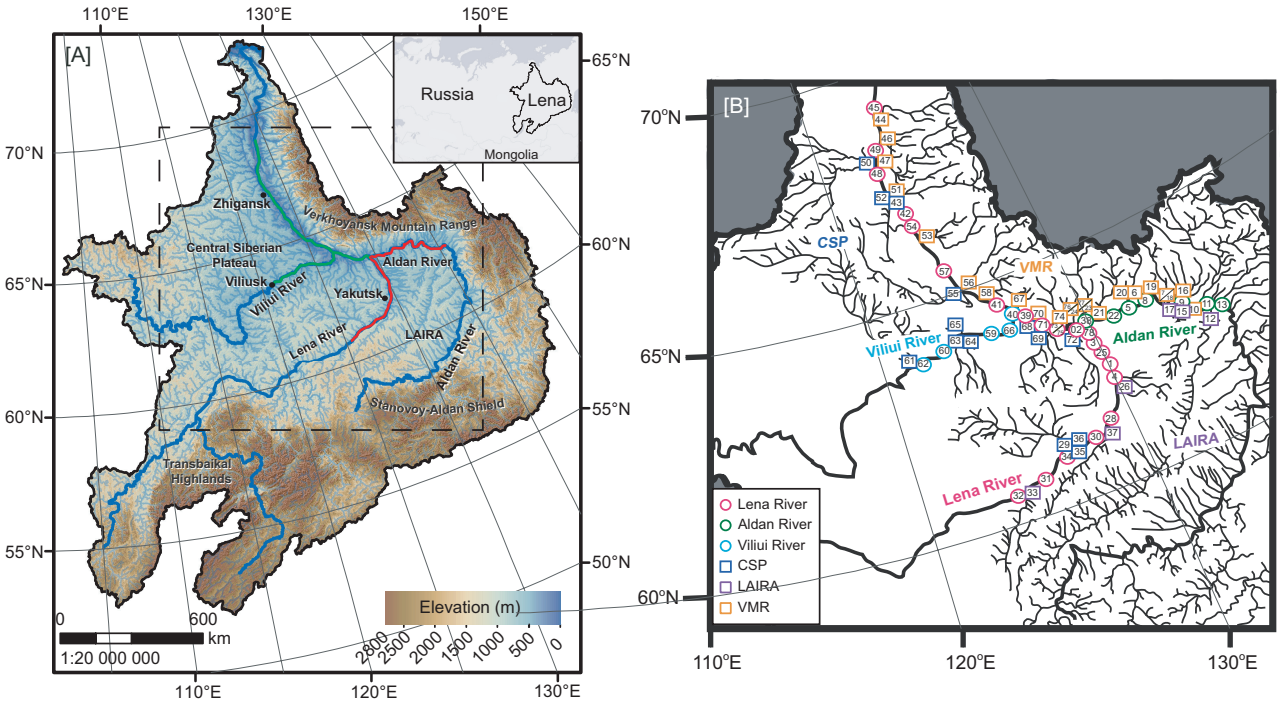

Figure 1: Map showing [A] the Lena River catchment and its sub-catchment regions with the July 2012 sampling route shown in red and June 2013 in green. Sampling locations are shown [B] with samples within the Lena River main channel or the Viliui and Aldan Rivers, which are major tributaries, denoted by circles. Smaller tributaries of the Central Siberian Plateau (CSP), Lena-Amginsky inter-river area (LAIRA) and Verkhoyansk Mountain Range (VMR) are denoted by squares (maps modified after Hirst et al. 2017).

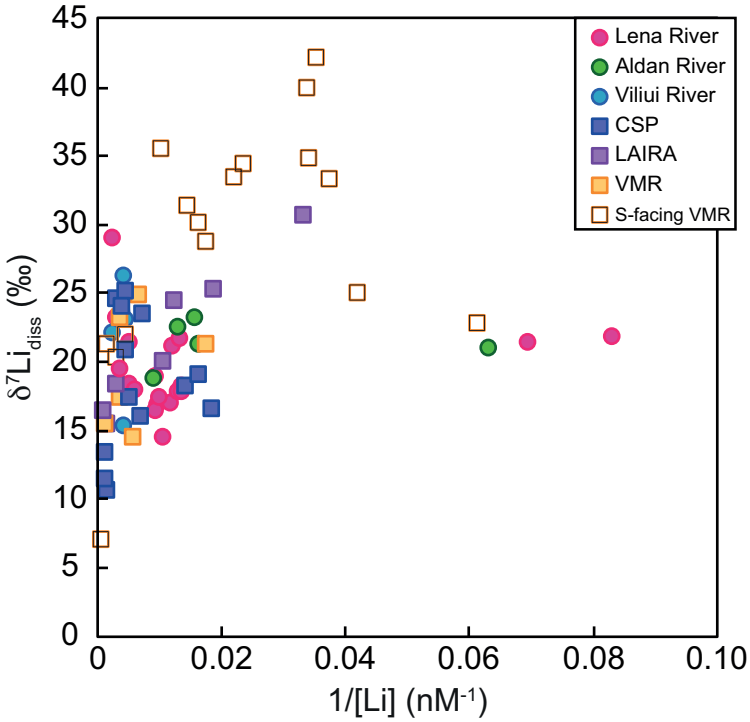

Figure 2: δ^7Li_{diss} compositions versus the inverse of dissolved Li concentrations for rivers in the Lena River watershed. Previous values from the Lena River watershed are shown for comparison (not shown is one anomalous sample UL436 that drains the evaporitic marine carbonates within the Siberian Platform with high [Li] of 3350 nM and δ^7Li_{diss} = 21.2‰(Huh et al., 1998a)). The range of values do not define clear, straight line mixing trajectories, thus are unlikely to be explained by simple mixing between two riverine end-members, and reflect the complex behaviour of Li in this watershed. Uncertainties on δ^7Li smaller than the symbols. CSP = Central Siberian Plateau; LAIRA = Lena-Amginsky inter-river area; VMR = Verkhoyansk Mountain Range. Open symbols represent VMR rivers draining south-facing catchments, which show the greatest variation in both [Li] and δ^7Li_{diss}.

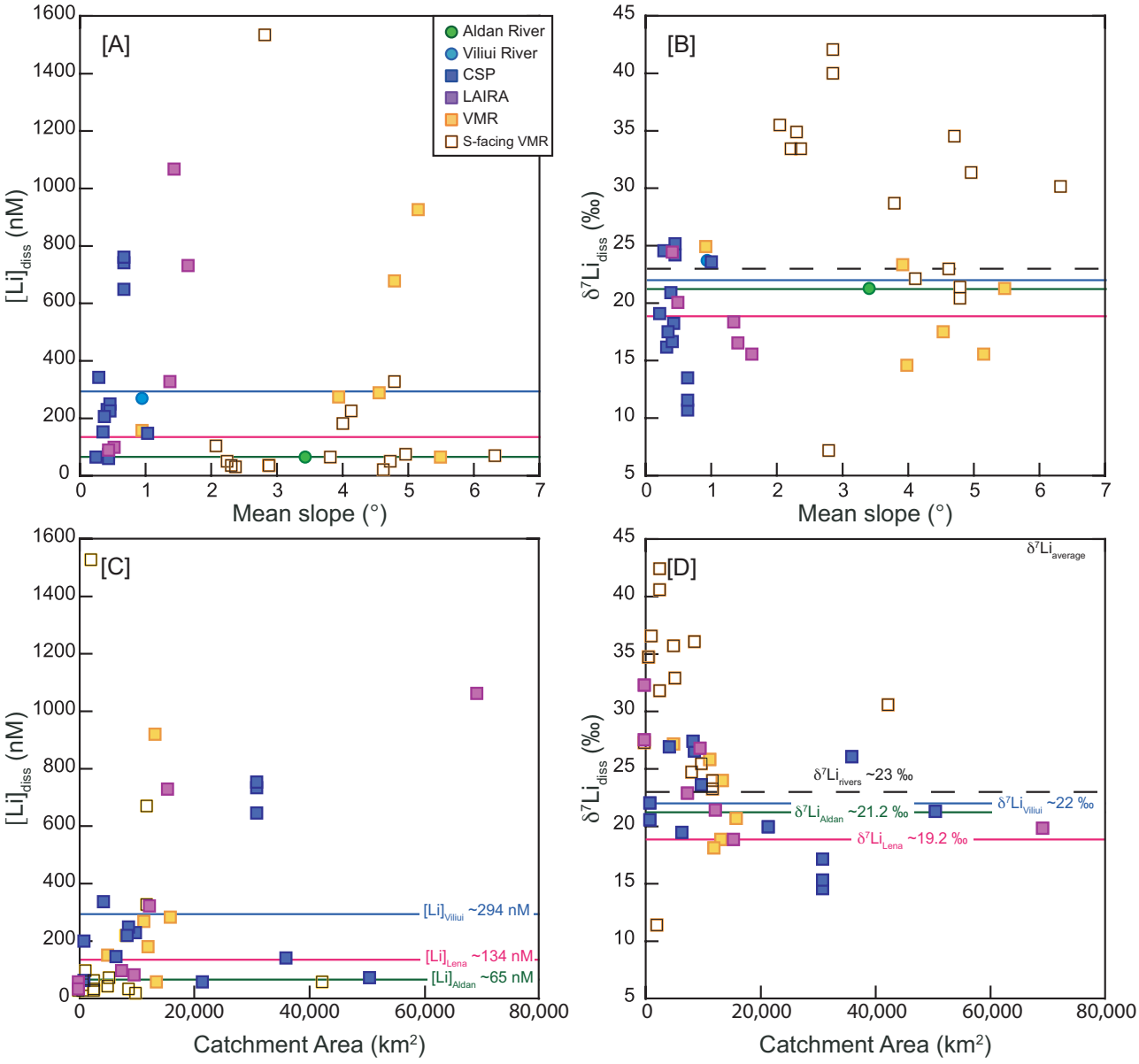

Figure 3: Dissolved Li concentrations and δ^7Li compositions compared with watershed gradient [A,B] and catchment area [C,D] for tributaries draining the Central Siberian Plateau (CSP), Lena-Amginsky inter-river area (LAIRA) and Verkhoyansk Mountain Range (VMR) regions. The lack of trends with watershed gradient may in part be a result of the unique cryogenic physical erosion processes associated with the presence of continuous permafrost, which obscure relationships observed in rivers draining high topography in non-permafrost rivers. The greatest variation in δ^7Li_{diss} compositions is seen in smaller (<10,000 km^2) catchment areas, particularly in rivers draining the south-facing catchments of the VMR (open symbols). Tributaries draining larger catchment areas tend to have δ^7Li_{diss} values closer to the global mean riverine value of 23‰ (shown as dashed line, after Huh et al. 1998a) as well as the average δ^7Li_{diss} compositions of the Lena, Aldan and Viliui Rivers (shown as solid lines in pink, green and blue respectively).

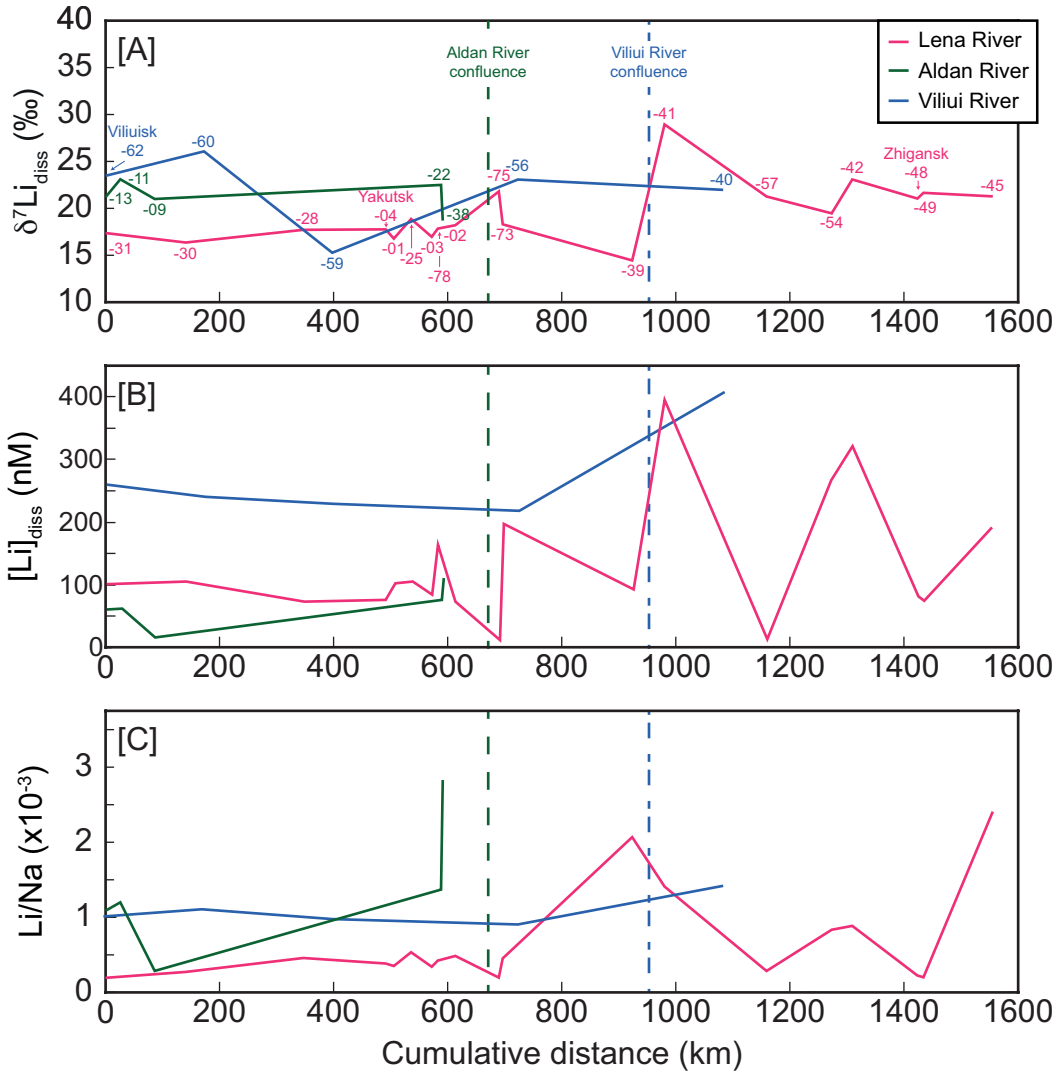

Figure 4: Downstream variations in δ^7Li_{diss}, [Li] and Li/Na in the Lena River main channel, and major tributaries of the Aldan and Viliui Rivers that converge into the main channel. River samples numbers are shown adjacent to curves, and arrows indicate the downstream river location of major towns. Confluences of the Aldan and Viliui Rivers into the Lena River main channel are shown as dashed lines. See Figure 1 for more information. No systematic trends can be observed in [Li], or Li/Na. A gradual ~5‰ increase can be seen along the Lena River main channel, see text for further details.

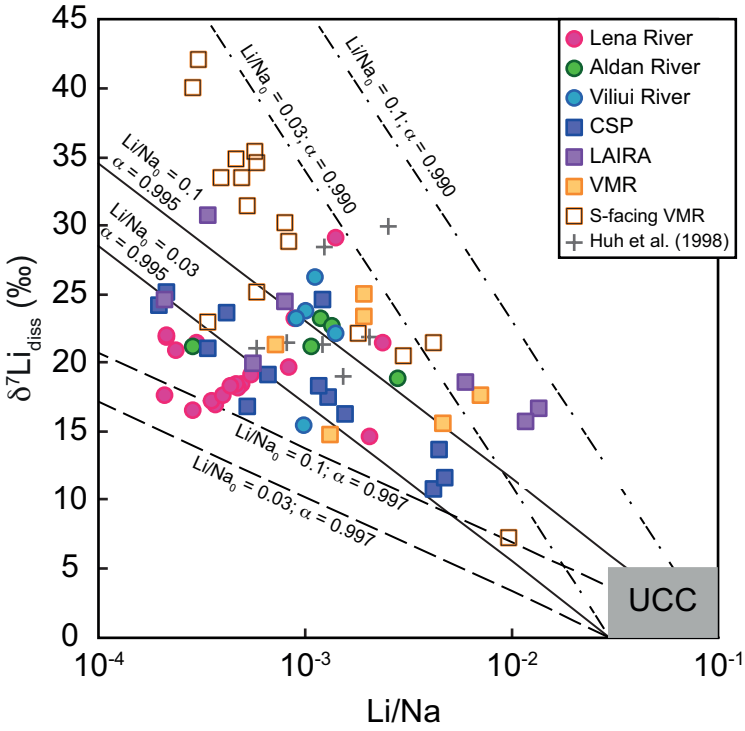

Figure 5: Relationship between measured δ^7Li_{diss} and Li/Na molar ratios for the Lena River. Shown for comparison are Lena River data from Huh et al. (1998a). The lines represent the evolution of δ^7Li and Li/Na following a Rayleigh distillation model, in which Li is supplied to waters by dissolution of primary silicate minerals, followed by the progressive removal of Li into secondary minerals. Curves are shown for different starting values and different fractionation factors for Li removal. The grey field represents the range of values that are generally expected for dissolution of silicate rocks, with Li/Na molar ratios between the highest measured in the Lena River watershed and the composition of upper continental crust (UCC), and δ^7Li values for UCC and typical shales (Taylor and McLennan, 1995; Teng et al., 2004; Dellinger et al., 2014; Sauzéat et al., 2015). CSP = Central Siberian Plateau; LAIRA = Lena-Amginsky inter-river area; VMR = Verkhoyansk Mountain Range. Open symbols represent VMR rivers draining south-facing catchments.

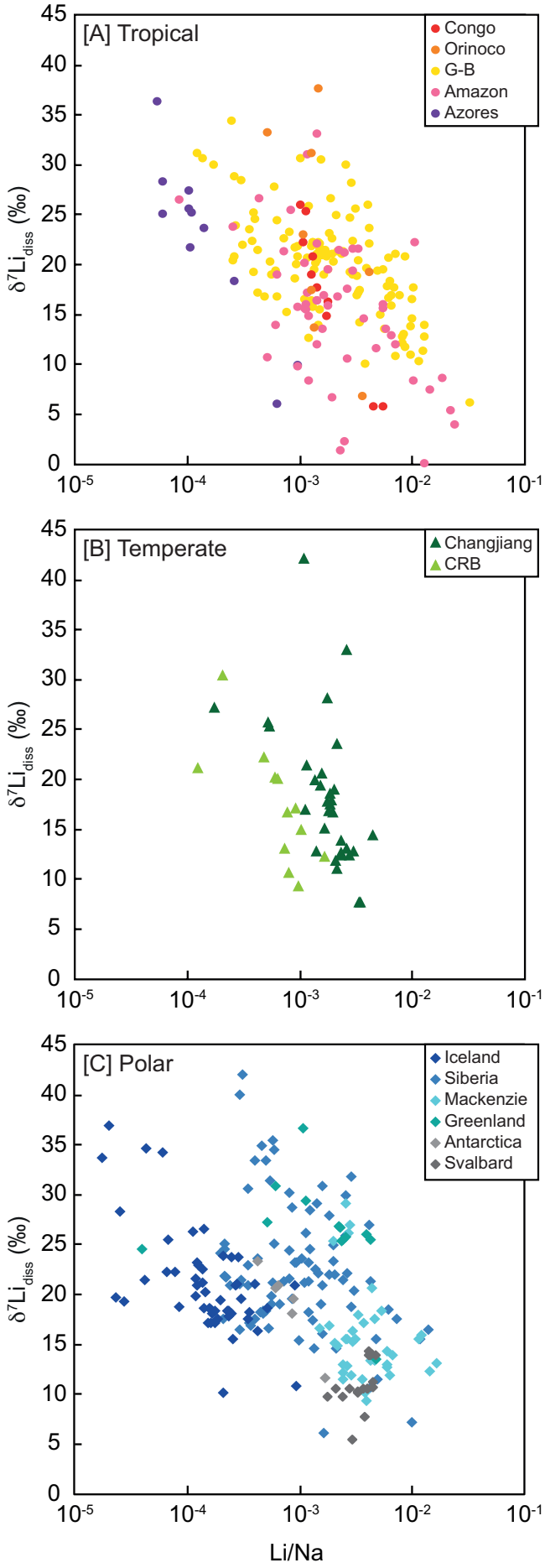
[A] Tropical
Congo
Orinoco
G-B
Amazon
Azores
[B] Temperate
Changjiang
CRB
[C] Polar
Iceland
Siberia
Mackenzie
Greenland
Antarctica
Svalbard
δ7Lidiss (‰)
Li/Na
0
5
10
15
20
25
30
35
40
45
10-5
10-4
10-3
10-2
10-1

1002

Figure 6: A compilation of dissolved Li isotope values versus molar Li/Na for rivers in [A] tropical, [B] temperate and [C] polar regions. Despite vastly different climatic and weathering regimes, the same range of riverine δ^7Li values globally suggests that cryogenic weathering features typical of permafrost-dominated regions and climate (temperature and runoff), are not a dominant control on δ^7Li fractionation. Data include the Lena River and other Siberian rivers (this study; Huh et al., 1998a); the Mackenzie River (Millot et al., 2003; Millot et al., 2010); Antarctic rivers (Witherow et al., 2010); Greenland (Wimpenny et al., 2010b); Svalbard (Hindshaw et al., 2016; Hindshaw et al., 2018); the High Himalayas (Huh et al., 1998a; Kısakűrek et al., 2005); the Ganges-Brahmaputra (Huh et al., 1998a; Kısakűrek et al., 2005; Bagard et al., 2015; Frings et al., 2015; Manaka et al., 2017; Pogge von Strandmann et al., 2017); the Amazon (Huh et al., 1998a; Dellinger et al., 2015); the Orinoco (Stallard et al., 1995;1996; Huh et al., 1998a); the Congo (Henchiri et al., 2016); Changjiang (Yangtzee) River (Huh et al., 1998a; Liu et al., 2011; Wang et al., 2015); and basalts from Iceland, the Azores and the Columbia River Basalts (Pogge von Strandmann et al., 2006; Vigier et al., 2009; Pogge von Strandmann et al., 2010; Liu et al., 2015).

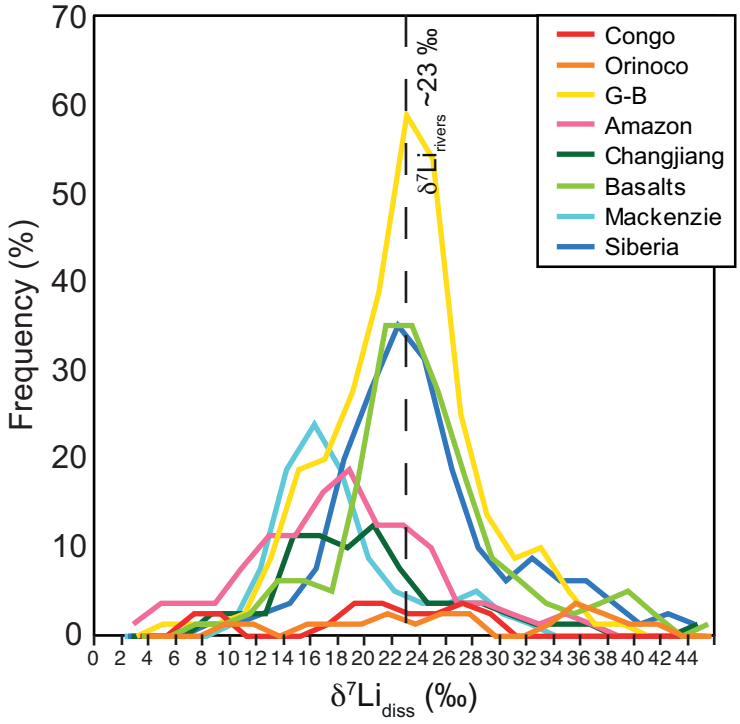

Figure 7: A two point moving average frequency histogram (2 permil bin width) summarising dissolved δ^7Li compositions from large global rivers, and rivers draining basaltic terrains. A large peak can be seen clustering around the global median value of 23‰ (Huh et al., 1998b), with a smaller peak around ~14 to 16‰. Data from same sources as Fig. 6.

Table 1: Field parameters and dissolved Li concentrations and dissolved and suspended particulate isotopic compositions of Lena River samples

Sample	Sampling date	Latitude	Longitude 'E	Mean slope (degree)	pH	Conductivity (us/cm^{C})	Na (µmol/L)	Li (nmol/L)	δ^7Li_{diss} (‰)	2sd	δ^7Li_{susp} (‰)	2sd
Aldan (Алдан) River												
LR2012-13 †	19/07/2012	62°38.296	134°55.313	3.44	7.7	86	56	61	21.2	0.7	2.2	0.7
LR2012-13 dup									20.9	0.7	2.8	0.7
LR2012-11	18/07/2012	62°42.635	134°41.712		7.3	99	52	63	23.1	0.7		
LR2012-09	18/07/2012	62°55.373	134°10.366		7.5	94	55	16	21.0	0.7		
LR2012-22	21/07/2012	63°26.290	129°40.001		6.8	105	55	76	22.5	0.7		
LR2013-38 †	12/06/2013	63°26.031	129° 38.390		7.4	86	39	112	18.7	0.7		
Central Siberian Plateau												
LR2012-29	25/07/2012	61°08.768	126°51.722	0.67	8.6	163	151	644	10.6	0.7		
LR2012-36	28/07/2012	61°10.079	126°52.061	0.67	9.4	171	162	732	13.4	0.7		
LR2012-35	28/07/2012	61°09.905	126°54.657	0.67	9.0	170	156	752	11.4	0.7		
LR2013-72	27/06/2013	63°28.065	128°47.392	0.42	7.4	201	653	225	20.8	0.7	5.1	0.7
LR2013-69	26/06/2013	63°58.454	127°01.742	0.47	7.5	346	1245	245	24.0	0.7	3.0	0.7
LR2013-68	26/06/2013	64°06.517	126°44.435	0.47	7.5	288	1007	217	25.0	0.7		
LR2013-61	23/06/2013	63°46.822	121°31.376	0.45	7.6	118	59	70	18.1	0.7	1.9	0.7
LR2013-63	24/06/2013	64°01.494	123°53.111	0.35	7.0	50	92	145	16.0	0.7		
LR2013-64	24/06/2013	64°01.658	124°05.540	0.3	8.4	159	270	334	24.5	0.7		
LR2013-65	24/06/2013	64°01.610	124°23.933	0.24	7.2	70	91	61	19.0	0.7		
LR2013-55	21/06/2013	64°57.121	124°35.775	0.43	6.7	58	102	54	16.6	0.7		
LR2013-43	14/06/2013	66°46.268	123°21.607	0.37	6.9	52	153	199	17.3	0.7		
LR2013-50	16/06/2013	67°52.577	123°02.186	1.04	7.1	134	333	139	23.5	0.7		
Lena-Amginsky inter-river area (LAIRA)												
LR2012-33	27/07/2012	60°35.619	124°16.356	1.65	8.2	305	61	725	15.5	0.7		
LR2012-37 †	29/07/2012	61°11.678	128 17.041		7.3	336	250	53	25.2	0.7	2.6	0.7
LR2012-37 dup									23.7	0.7		
LR2012-27	24/07/2012	61°15.061	128°46.172	1.37	8.0	310	53	320	18.3	0.7		
LR2012-27 dup									18.5	0.7		
LR2012-26 †	24/07/2012	61°54.233	129°50.831	0.52	7.2	106	166	93	19.9	0.7	4.6	0.8
LR2012-26 dup									19.5	0.7		
LR2012-12	19/07/2012	62°36.881	134°55.373	1.43	8.2	299	77	1061	16.4	0.7	4.0	0.7
LR2012-15	19/07/2012	62°56.787	134°00.503		6.5	145	87	30	30.5	0.9		
LR2012-17	20/07/2012	63°01.219	133 24.489	0.43	7.4	133	101	81	24.3	0.7		
Lena (Лена) River Main Channel												
LR2012-31	26/07/2012	60°52.334	125°38.010		7.22	-	481	101	17.4	0.7		
LR2012-31 dup									17.5	0.8		
LR2012-30	25/07/2012	61°06.475	126°53.429		7.7	125	368	106	16.4	0.7		
LR2012-28	24/07/2012	61°15.823	128°44.383		7.47	80	154	73	17.7	0.7		
LR2012-28 dup									18.2	0.7		
LR2012-04 †	14/07/2012	62°09.462	129° 54.481		6.63	81	191	77	17.8	0.7	1.6	0.7
LR2012-04 dup									17.2	0.7	1.4	0.7
LR2012-01	12/07/2012	62°15.758	130° 01.031		6.82	90	281	103	16.8	0.7		
LR2012-25	22/07/2012	62°38.949	129°54.446		6.86	90	192	106	18.9	0.7		
LR2012-03	13/07/2012	63°01.161	129° 41.079		6.52	84	237	85	17.0	0.7		
LR2013-78	28/06/2013	63°07.960	129°37.392		7.58	139	375	165	17.9	0.7		
LR2013-78 dup									18.4	0.7		
LR2012-02 †	12/07/2012	63°23.275	129° 32.356		6.57	69	146	73	18.2	0.7	2.6	0.7
LR2012-02 dup											2.5	0.7
LR2013-75 †	27/06/2013	63°31.690	128°51.598		7.56	92	56	12	21.8	0.7		
LR2013-73 †	27/06/2013	63°29.425	128°48.183		7.3	142	420	197	18.3	0.7		
LR2013-39 †	12/06/2013	64°13.095	126°51.861		7.57	101	45	94	14.5	0.7		
LR2013-41	13/06/2013	64°23.668	126°21.951		7.03	140	277	396	29.0	0.7		
LR2013-57 †	21/06/2013	65°03.067	124°48.330		6.99	83	48	14	21.3	0.7		
LR2013-54	19/06/2013	65°56.914	123°54.840		7.06	128	315	268	19.5	0.7		
LR2013-42	14/06/2013	66°20.636	123°40.556		7.29	139	356	322	23.1	0.7		
LR2013-48	16/06/2013	67°52.424	123°05.536		7.11	121	340	82	21.1	0.7		
LR2013-48 dup									20.5	0.7		
LR2013-49	16/06/2013	67°55.744	123°00.123		7.02	130	344	75	21.7	0.7		
LR2013-45	15/06/2013	68°44.599	123°59.794		7.09	91	79	192	21.3	0.7		
Viliui (Вилюи)												
LR2013-62	23/06/2013	63°45.493	121°35.897	0.96	7.4	111	254	261	23.5	0.7		
LR2013-60	23/06/2013	63°54.536	123°08.739		7.2	110	215	241	26.1	0.7	3.6	0.7
LR2013-59 †	22/06/2013	63°52.202	125°10.004		7.2	110	232	230	15.3	0.7		
LR2013-66	24/06/2013	64°03.180	126°04.148		7.4	112	238	220	23.1	0.7		
LR2013-40	13/06/2013	64°19.678	126°22.321		7.2	140	285	409	22.0	0.7		
Verkhoyansk Mountain Range												
LR2012-10 †	18/07/2012	62°38.249	134°54.869	3.82	7.0	148	67	57	28.6	0.7		
LR2012-16 †	20/07/2012	63°06.195	134 02.301	2.32	6.3	103	63	29	34.7	0.9	0.4	0.7
LR2012-07 †	17/07/2012	63°12.264	133°14.042	4.73	7.0	168	73	42	34.3	1.2		
LR2012-18	20/07/2012	63°022.064	133 016.417		6.6	118	41	24	24.9	0.7		
LR2012-19 †	20/07/2012	63°23.152	133°08.212	2.38	6.6	50	68	27	33.2	0.7		
LR2012-06 †	16/07/2012	63°19.254	131°55.854	6.34	7.4	206	77	62	30.0	0.8		
LR2012-20 †	20/07/2012	63°21.350	131°45.191	2.24	6.8	60	91	45	33.3	0.7		
LR2012-21	21/07/2012	63°20.639	130°22.743	4.13	7.0	244	119	216	22.0	0.7		
LR2012-23	21/07/2012	63°27.689	129°34.158	4.81	7.1	170	106	322	20.3	0.7		
LR2013-77	28/06/2013	63°28.084	129°35.651	4.81	7.6	206	158	668	21.2	0.7		
LR2012-24 †	21/07/2012	63°31.213	129°23.987	2.88	6.8	50	102	29	39.8	0.7		
LR2013-76 †	28/06/2013	63°31.325	129°23.775	2.88	7.5	49	92	28	41.9	0.7		
LR2013-74 †	27/06/2013	63°31.216	128°49.910	4.98	7.8	93	129	69	31.2	1.0		
LR2013-70	26/06/2013	64°01.146	127°21.009	2.08	7.4	88	168	97	35.4	0.7		
LR2013-70 dup									35.2	0.7		
LR2013-67 †	26/06/2013	64°09.811	126°57.998	2.82	7.2	73	156	1524	7.1	0.7		
LR2013-58 †	22/06/2013	64°36.009	125°43.076	4.64	7.1	89	47	16	22.8	0.7		
LR2013-56	21/06/2013	65°00.332	124°56.650	5.17	7.3	178	195	917	15.4	0.7		
LR2013-53	18/06/2013	66°13.971	124°09.683	4.01	7.2	159	134	178	14.5	0.7		
LR2013-51	17/06/2013	67°15.126	123°24.505	5.5	7.4	140	79	57	21.2	0.7		
LR2013-47	16/06/2013	68°01.293	123°24.905	4.57	7.1	104	39	281	17.4	0.7		
LR2013-46	15/06/2013	68°23.313	123°58.426	0.94	7.1	64	77	151	24.8	0.7		
LR2013-44	15/06/2013	68°43.951	124°03.581	3.94	7.2	182	136	267	23.2	0.7		

**Sampling stations are listed from upstream to downstream

Mean slope angle for upstream Lena River main channel sample LR2012-32 (not measured for [Li] or δ7Lidiss) is 3.2°. See Kutscher et al. (2017).

† Samples had [Li] below detection on the element 2, so [Li] were estimated by intensity matching against a known concentration of L-SVEC on the MC-ICP-MS, with uncertainties estimated at ± 10 %

VMR samples LR2012-10 to LR2012-23 and LR2012-77 to LR2103-58 are rivers draining south-facing catchments. See main text.